KINETIC AND THERMODYNAMIC ANALYSIS OF COMBINED DRY, STEAM AND PARTIAL OXIDATION REFORMING OF METHANE

A Thesis

by

MOHAMED SUFIYAN AZIZURREHMAN CHALLIWALA

Submitted to the Office of Graduate and Professional Studies of
Texas A&M University
in partial fulfillment of the requirements for the degree of

MASTER OF SCIENCE

Chair of Committee,	Nimir O. Elbashir
Co-Chair of Committee,	Patrick Linke
Committee Member,	Khalid Qaraqe
Head of Department,	M. Nazmul Karim

May 2016

Major Subject: Chemical Engineering

ABSTRACT

Dry reforming of methane is one of the few chemical reactions which can effectively convert carbon dioxide (CO_2), a major green-house gas, into a valuable chemical precursor, syngas (a mixture of CO and H_2), that can be converted into chemicals and fuels via different synthesis routes such as the Fischer Tropsch synthesis. The inherent limitations of dry reforming reaction, for instance, rapid catalyst deactivation by coke deposition and the very high energy requirements, has restricted its use as a commercial technology. This study was performed to evaluate the potential of overcoming the limitations of dry reforming by integrating it with other commercial methane reforming technologies such as steam reforming and partial oxidation reforming in the context of industrial operating conditions. A thermodynamic and kinetic analysis of the combined reforming has been conducted using the software suite MATLAB®. The aim of this complicated assessment is to identify optimized combination of the three reformers and also the corresponding operating conditions that would utilize significant amount of CO_2 while ensuring CO_2 fixation, minimum carbon formation and optimum energy requirements. The thermodynamic equilibrium product distribution calculations involved the Peng Robinson (PR), Redlich Kwong (RK) and Soave Redlich Kwong (SRK) equations of state (EOS) to identify the best EOS that accounts for the non-ideality associated with the high pressure operation. The study evaluated simultaneous effects of temperature (200 ^oC to 1200 ^oC), pressure (1 to 20 bar) and feed mole ratios (of methane, steam, carbon dioxide and oxygen) on the equilibrium product distribution. The addition of oxygen and steam to dry

reforming helped in decreasing energy requirements while simultaneously increasing the syngas yield ratio (H_2:CO ratio). The numerical evaluation revealed an optimized operating condition of ~750 ^oC at 1 bar pressure at a feed mole ratio CH_4: H_2O: O_2: CO_2 of 1:0.4:0.3:1. For this optimization, the system boundaries were limited only to a reformer block without considering the upstream and downstream processes. At this optimized condition, the carbon deposition was eliminated and the CO_2 conversion was observed to be 52% with an energy requirement of 180 kJ. The study is further extended to include kinetic analysis of combined dry and steam reforming of methane. The preliminary findings of kinetic evaluation indicated an excellent agreement between combined kinetic models with the thermodynamic equilibrium results. This work thus lays a foundation for the experimental investigation which will be aimed at the development of a very noble class of catalysts that will be able to resist carbon deposition in a dry reforming process.

DEDICATION

Dedicated to my family.

ACKNOWLEDGEMENTS

In the name of God, most gracious, most merciful.

I would like to show my extreme sense of gratitude to my committee chair, Dr. Nimir Elbashir for his consistent motivation and support through the course of this research, whose guidance and support aided me in writing this Thesis. I would like to thank my committee co-chair, Dr. Patrick Linke and committee member Dr. Khalid Qaraqe for their guidance and support during the course of this research. I would also like to thank Dr. Mohammed Minhaj Ghouri, who has always remained with me in all the nooks and crannies of this work constantly inspiring me with new ideas without which I would not have been able to achieve the results of this work.

I would also like to acknowledge my friends, colleagues and the department faculty for their continuous help and support whenever I needed during my time in the University which was made an extremely great experience. I also want to extend my gratitude to the entire research team of Dr. Elbashir specifically Dr. Hanif Chaudhury and Mr. Anuj Prakash, who always helped me in all the times of need. Lastly but not the least I want to thank my Parents and other family members for their love and support throughout my study.

GLOSSARY

GHG	Greenhouse gasses
DRM	Dry reforming of methane
SRM	Steam reforming of methane
POX	Steam reforming of methane
CRM	Combined reforming of methane
FTS	Fischer Tropsch synthesis
EOS	Equation of state
RK	Redlich Kwong
SRK	Soave Redlich Kwong
PR	Peng Robinson
P	Pressure of the reaction system (bar)
T	Temperature of the reaction system (K)
P^o	Standard pressure of 298 K
R	Universal molar gas constant ($\frac{J}{mol.K}$)
GFE	Gibbs free energy
G^{total}	Total Gibbs free energy ($\frac{J}{mol}$)
$\Delta G_{fi}{}^{o}$	Standard Gibbs free energy of formation of specie i ($\frac{J}{mol}$)
n_c	Number of moles of solid carbon (mol)
y_i	Mole fraction of specie i
Ak	Total mass of element k
a_{ik}	Number of atoms in element k
$n_{i,exit}$	Number of moles in stream leaving the reformer (mol)
$H_{i,exit}$	Enthalpy of stream leaving the reformer ($\frac{J}{mol}$)
$H_{i,feed}$	Enthalpy of stream entering the reformer ($\frac{J}{mol}$)
Z	compressibility factor
μ_i	Chemical potential of specie i
$\hat{\varphi}_i$	Fugacity coefficient of specie i
λ_k	LaGrange's undetermined multiplier

TABLE OF CONTENTS

Page

LIST OF TABLES

Page

LIST OF FIGURES

Page

CHAPTER I

INTRODUCTION

Natural gas, which mainly comprises of methane (80-97 volume %) is converted to syngas (a mixture of hydrogen (H_2) and carbon monoxide (CO)) by a process known as Reforming. Historically, reforming process was recognized to be industrially important when mass production of ammonia started in 1913. Significance of reforming was then attributed to its capability of producing hydrogen (H_2) on an extremely large scale as H_2 was a basic raw material for the production of ammonia. Later, after the invention of Fischer Tropsch process by german scientists Franz Fischer and Hans Tropsch in 1925, reforming process started getting more attention as the direct product of reforming (syngas) is used for Fischer Tropsch synthesis. Syngas is a valuable precursor for the production of clean fuels via the Fischer-Tropsch Synthesis (FTS) [1, 2] and chemicals such as alcohols. Syngas is also attractive in inducing integration among different manufacturing facilities that are located in the same industrial city or coupled through an eco-industrial park [3]. Steam reforming of methane (SRM) is known to be the oldest and the most widely used type of reforming process. In this process, high temperature steam reacts with preheated methane to produce syngas.

Steam Reforming of Methane (SRM)

$$CH_4 + H_2O \rightleftarrows CO + 3H_2 \qquad \Delta H_{298} = 206 \text{ kJ/mol} \qquad (1)$$

Other type of reforming process include the Dry Reforming (DRM) and the Partial Oxidation Reforming processes (POX). The need for effective utilization and conversion of the carbon dioxide (CO_2), which is a major greenhouse gas (GHG), emphasizes the

interest in the DRM reaction. DRM is a process in which carbon dioxide and methane react to form syngas.

Dry Reforming of Methane (DRM)

$$CH_4 + CO_2 \rightleftarrows 2CO + 2H_2 \qquad \Delta H_{298} = 247 \text{ kJ/mol} \qquad (2)$$

In contrast to SRM and DRM which are highly endothermic, POX is an exothermic process [4, 5]. Partial oxidation is the only reforming process which can also be conducted without the presence of a catalyst [6]. The downstream processes in which the produced syngas is to be utilized dictates the appropriate methane reforming technology; for instance, FTS with a cobalt based catalyst requires the synthesis gas yield ratio (H_2:CO) of 2:1.

Partial Oxidation of Methane (POX)

$$CH_4 + \tfrac{1}{2}O_2 \rightleftarrows CO + 2H_2 \qquad \Delta H_{298} = -36 \text{ kJ/mol} \qquad (3)$$

Although, in principle, the energy required to drive the SRM and DRM may be provided from various sources including fossil fuels, solar energy, and other renewable sources, fossil fuels are currently most commonly used. Such usage leads to further GHG emissions associated with combustion of fossil fuels. The adoption of DRM presents a very pragmatic route of CO_2 utilization for an economy such as the state of Qatar, which has one of the world's largest per capita CO_2 emissions rate [7]. Nonetheless, DRM still faces acute issues in the practical implementation because of its inherent process limitations. Among these is the formation of sufficient amounts of carbon that leads to a rapid deactivation of the catalyst [8, 9]. This is further complicated by high energy requirements that amount to almost 1.2 times that of the SRM. Another serious

consideration for DRM is the problem of low-quality syngas in terms of its hydrogen to carbon monoxide yield ratio (H_2:CO ratio of ≤1). Despite the fact that cobalt based FTS requires syngas with an H_2:CO ratio of 2:1, CO-rich syngas produced from DRM increases the selectivity of long chain hydrocarbons, Dimethyl-Ether (DME) and methanol in direct syngas conversion routes [2, 5, 10]. Due to these challenges, dry reforming is still a 'gray' area demanding more attention from the scientific community.

In the literature, the issues related to the practical implementations of DRM have been suggested to be addressed by synergistically combining the DRM, SRM and POX reforming into a Combined Reforming of Methane (CRM) process [11-13]. Previously in our group, Noureldin et al. [11] reported the comparison between the three reforming techniques in terms of their syngas quality, energy requirements, and operating conditions. They suggested the combined operation of these reforming techniques with their potential benefits in view of CO_2 fixation. The same authors in a later study [14] also presented a realistic quantification of the CO_2 fixation using DRM process via integration of the conventional reforming technologies. They also highlighted the important tradeoffs associated between the CO_2 chemical fixation and its effect on the syngas yield ratio. On a very similar note, Jonas et al. [15] presented a comparative study of a set of five alternative combined reforming routes which compete with DRM process on an annual total cost basis and they demonstrated that DRM/SRM process requires minimum total annual cost. Luyben et al. [16] reported a practical dynamic modeling study highlighting the major tradeoff that could be expected during standalone operation of the DRM process. Özkara-Aydınoğlu et al. [12] analyzed different operating scenarios of the combined

SRM/DRM by tuning the reformer feed mole ratio and reported that the activity of methane and H_2:CO yield ratio increases considerably upon addition of steam to DRM. Zhang et al. [17] studied the effect of varying the feed mole ratio on the product distribution and proposed an optimum feed ratio (CH_4: CO_2: H_2O: O_2 = 1: 0.291: 0.576: 0.088) to maximize H_2 yield and CO_2 conversion, while maintaining a desired (H_2:CO) yield ratio for the downstream methanol synthesis. Chein et al. [18] performed thermodynamic study of the effect of addition of inert gas on the product distribution of the DRM process and reported that the reactant conversion drops significantly due to the presence of inert gases. They also studied the combined performance of DRM/POX and DRM/SRM bi-reforming processes in view of suppressing carbon formation in single DRM process. Amin et al. [19] reported an optimum feed mole ratio (CO_2:CH_4:O_2=1:1:0.1) in view of reducing reforming temperature, while maximizing H_2 yield and CO_2 conversions. Thermodynamic analysis was also performed by Nematollahi et al. [13] and they reported that pressure has inverse effect on methane conversion in combined POX/DRM reforming of methane. Nikoo et al. [20] carried out similar analysis of carbon formation in a DRM process, and they observed that high pressure operation suppresses the effect of high temperatures on reactant conversions and results in an increased carbon formation. They also carried out a comparison between the experimental and thermodynamically calculated results to study the differences between the real and thermodynamic equilibrium profile in a DRM process.

As reported from the previous studies, the parameters that control the operation of the CRM process are not only temperature and pressure conditions but also the feed mole

ratios [21-24]. In this study, we have taken a base case scenario of CH_4: H_2O: O_2: CO_2 feed ratio of 1: 0.6: 0.1: 0.6. This ratio can be approximated to the flue gas composition which can potentially act as a possible feed to the CRM reactor [25].

The challenge related to carbon formation is hypothesised to be addressed in either of the two ways:

(a) by introducing either steam, oxygen or both in the feed (i.e., replacing DRM with a CRM process) or,

(b) by developing novel catalysts that can either work effectively in coke environment or resist the formation of coke layers on its surface. Choudhury et al. [26] reported a rare-earth element Neodymium (Nd)/Cobalt (Co) based catalyst that could prevent itself from carbon deposition. Later, same authors demonstrated the utility of this catalyst for CRM at different process conditions [27].

The effect of addition of oxygen to reduce carbon formation was reported by Song et al. [25], who were amongst the first ones to perform an experimental study on the CRM process, they used flue gas samples as feed to the CRM process and observed that carbon formation occurs in relatively much lower quantities compared to the DRM process. A similar study was also done by Lee et al. [28], the objective of their study being to produce syngas for DME synthesis. They observed that carbon deposition can be suppressed by using coke resistant catalysts and by introduction of oxidant like steam and oxygen in the DRM process. More recently, synthesis gas production for FTS using CRM process has gained immense attention owing to many advantages this process offers compared to the conventional reforming processes.

Much of the research work previously considered the reaction mixture at the reformer operating conditions to be ideal mixture [11, 13, 18, 29]. However, non-ideality could be expected due to high-pressure and high-temperature conditions. In this work, the effect of non-ideality in the reaction mixture has been accounted for by incorporating the fugacity coefficients calculated using Redlich-Kwong(RK), Soave-Redlich-Kwong (SRK) and Peng-Robinson (PR) equations of state (EOS).

One of the major short comings of the DRM is related to the high energy requirements associated with this process. The energy costs associated with the reforming process directly influences the overall downstream costs such as the Gas to Liquid (GTL) products cost. Minimizing this cost could present an excellent opportunity to lower the costs of the energy intensive GTL technology since the cost of reforming process is between 60-70% of the GTL plant operating cost. A precise analysis with regards to the energy requirement assessment is inevitable to be able to overcome this shortcoming. While there have been numerous studies, both experimental as well as modeling, reported in the literature, which address coke deposition as well as low syngas quality of DRM products, only Noureldin et al. [11] briefly addressed the subject of energy requirements for this technology. An extensive energy analysis is an integral part of this work and the amount of energy required to sustain various process conditions is used as a major criteria to comment on the merit of the said conditions.

In addition to the thermodynamic modeling of CRM, we performed Kinetic analysis of combined DRM/SRM process. One of the well-established kinetic model for SRM has been reported by Xu et al. [30]. They have derived a Langmuir-Hinshelwood

Hougen-Watson (LHHW) kinetic rate expression for SRM on a nickel based catalyst ($Ni/MgAl_2O_4$). Verikyos et al. [31] have published a kinetic model for DRM reaction (also for a nickel based catalyst (Ni/La_2O_3)). There are also other such kinetic models which relatively accurately describe the behavior of individual reforming processes [32-35]. In the present work, we have made an attempt to consolidate together the individual SRM and DRM models proposed by Xu et al. [30] and Verykios et al. [31] respectively. The benefits of using such a model are numerous; the combined model represents a coupled entity of already established models, so there will be no need for an additional model for a specific system, also this extends the applicability of the individual model quite effectively. The other advantage of the combined model could be its applicability in representing a combined reforming process in simulation studies, which are generally carried out before conducting expensive experimental studies. The combined kinetic model could also be utilized in designing of new reactors and to estimate the probable outcome of an experiment for better process control. The model can also be used in catalyst scale up studies for industrial reactors. In the current work, we have used this coupled model to evaluate the kinetics of combined DRM/SRM process. We have compared the product distribution of a combined DRM/SRM process using this coupled kinetic model to the product distribution predicted by our equilibrium thermodynamic calculations in order to validate the coupled kinetic expressions. This facilitated us to identify the regions of kinetic deviations from the thermodynamic equilibrium results.

While there have been numerous studies, as discussed above, which explore the thermodynamic equilibrium of the combined reforming process, the importance of the

present work is that it validated the thermodynamic results against the well-established reaction kinetic models, which provide an excellent opportunity to design more effective catalytic systems for the DRM process.

CHAPTER II

RESEARCH OBJECTIVE

In the previous studies, as mentioned in chapter 1, most of the work on the reforming study by thermodynamic analysis was carried out based on the assumption that the reformer reaction mixture is an ideal mixture. However, in the present study we considered both ideal and non-ideal behaviors of the reaction mixture. Non ideal conditions arise at high pressure operations, which is the typical operating condition for most industrial reformers. In order to evaluate the potential of DRM as an economical reforming process compared to the conventional reforming processes, this study has been carried out in two steps: first, a detailed thermodynamic study that helps to evaluate the effect of the different process variables (temperature, pressure and feed mole ratios) was conducted for the combined DRM/SRM/POX process. Second, this study has been extended to involve as well kinetic analysis of the combined DRM/SRM process. As a first step to evaluate kinetics of a DRM/SRM process, efforts were made to develop combined DRM/SRM model based on the existing Kinetic models in literature. The thermodynamic and kinetic analysis as mentioned above was carried out for the following objectives:

1) DRM reaction, as highlighted in chapter 1 (page 1), faces some very critical process limitations of coke deposition and high endothermicity with a low quality of syngas yield ratio. One of the major objectives of this study is to evaluate the potential of utilization of the combined DRM/SRM/POX reforming of methane to tackle the aforementioned DRM process limitations.

2) By using thermodynamic principle of Gibbs free energy minimization, this study is aimed at exploring the possibility of optimizing the different process variables (temperature, pressure and feed mole ratios) that effect the behavior of the reformer. Minimization of the carbon deposition, energy requirements, and improvement of the syngas yield ratio are the three optimization parameters that have been targeted in this study.
3) The parameters that control the operation of the CRM process are not only temperature and pressure conditions but also the feed mole ratios [21-24]. In this study, our aim is to use a base case scenario of CH_4:H_2O:O_2:CO_2 feed ratio of 1:0.6:0.1:0.6. (as this approximates to flue gas composition which can potentially act as a suitable feed to the CRM reactor [25]), and to utilize this feed condition for further optimization of all the process conditions.
4) Thermo-equilibrium analysis of reforming captures the interdependency of the different operating conditions. It serves to be a good starting point for understanding the feasibility of the system as well as its behavior under different operating conditions. In the present work, a complete thermodynamic equilibrium analysis of the CRM process has been carried out to evaluate the behavior of the system under non-Ideal conditions. In particular, energy economy, non-ideality and the syngas (H_2: CO) yield ratio under different process conditions will be studied. These aspects will be utilized to address the limitations of a DRM process in view of CO_2 fixation, minimization of carbon deposition and energy minimization.

5) Another important objective of this study is to analyze the behavior of the combined reforming of methane, this work is also aimed at the integration of the existing Steam and Dry reforming Langmuir-Hinshelwood-Hougen-Watson Kinetic models, into a combined DRM/SRM kinetic model. This task, is to cater to the fact that, there is no particular kinetic model for the combined DRM/SRM system.
6) This research is also aimed at studying the regimes of kinetic deviation from the feasible equilibrium predictions when the evaluation is based on thermodynamic analysis of the combined DRM/SRM process.
7) To verify the developed Kinetic model capabilities this study we tested the model predictability for a pseudo homogeneous fixed bed reactor. The simulated reactor model will also serve as a platform for carrying out pre-experimental analysis for the future experimental catalyst scale up studies.

CHAPTER III

RESEARCH METHODOLOGY

As mentioned earlier in chapter 1 (page 1), the present study has been divided into thermodynamic analysis and kinetic analysis separately. The thermodynamic study is based on equilibrium calculations which is mentioned in detail further in section 3.1 (page 12). Kinetic study however is based completely on kinetic modeling and integration of the existing kinetic models available in the literature, this is mentioned in detail in section 3.2 on kinetic calculations (page 19). The kinetic analysis is also further divided into model integration and fixed bed reactor modeling work separately. The Matlab code® developed for both the thermodynamic and kinetic studies is also shown in Appendix A (page 78).

3.1 Thermodynamic Calculations

Evaluation of the equilibrium composition of a general multi-reaction and multi-component mixture requires the utilization of the principle of Gibbs Free Energy (GFE) from the fundamentals of thermodynamics. GFE is the free energy available in the system to do useful work. At a condition of chemical reaction equilibrium, the GFE of the system is minimum which indicates that no more additional work can be done by the system which means that the system is at dynamically stable condition. The multi-reaction equilibrium calculation is carried out thus by minimizing the GFE of the system. GFE is a function of temperature, pressure and molar composition of the species present in the system. Equilibrium product distribution at a given process condition is obtained by identifying the relation between these process variables and then tuning one of the process variable by limiting the degree of freedom of the system to one. By conducting such calculations

for all the three process variables, optimum operating scenarios could be identified subject to specified constraints.

Following steps adopted from Abbot et al. [36] shows the calculation philosophy of a general GFE minimization process:

Step 1:

At a given condition of temperature and pressure, the Gibbs energy of an N component system is given by:

$$(G^{total})_{T,P} = f(n_1, n_2, n_3, n_4 \ldots\ldots n_N) \quad (4)$$

Now, the problem is to find a set of (n_i) moles of the given components which minimizes the G^{total} for a specified temperature T, and pressure P. this equation will also be subjected to material balance across the chosen system. The most common solution to this type of problem is to convert the governing equations to a set of nonlinear equations by introducing Lagrange's undetermined multipliers. These additional parameters serves to act as dummy variables which would be needed to convert the problem to an easily solvable system of nonlinear equation, though these variables themselves do not hold any significance in relation to the system.

Step 2:

The second step is to identify the constraint equations, which in this case are the material balance equations. It should be noted that the reaction molecular system is not conserved in a closed system, but the total number of atoms of each element will always be conserved according to the principle of conservation of mass.

If A_k and a_{ik} denote the total number of atomic masses and number of k^{th} element in each molecule respectively, the material balance for k^{th} element can be given by:

$$\sum_i n_i \, a_{ik} = A_k \quad (5)$$

or;

$$\sum_i n_i a_{ik} - A_k = 0 \quad (6)$$

Step 3:

The next step is to introduce the Lagrange's multiplier for each element in the mass conservation equation:

$$\lambda_k(\sum_i n_i a_{ik} - A_k) = 0 \quad (7)$$

Where, λ_k represents the Lagrange's multiplier pertaining to each element k.

Step 4:

In order for the GFE equation (4) to comply with the conservation equation (7), both the equations are solved simultaneously by addition of the GFE equation to the conservation equation as shown below:

$$G^{total} = \sum_{i=1}^{N} n_i \mu_i \quad (8)$$

Where, n_i is the number of moles of component *i* that has a chemical potential μ_i. N is the total number of components in the system. The chemical potential of species *i* can be defined as:

$$\mu_i = \Delta {G_{fi}}^o + RTln\left(y_i \hat{\varphi}_i \frac{P}{P_o}\right) \quad (9)$$

where ΔG_{fi}^0 is the standard Gibbs energy of formation for specie *i*. *R* is the universal molar gas constant, *T* is the absolute temperature, y_i is the mole fraction of species *i*. $\hat{\varphi}_i$ is the fugacity coefficient of species *i* calculated using the pertinent equation of state. *P* is

the operating pressure and P_o is the standard pressure of 298 K. Substituting equation (9) in (8), we get the expression for GFE as:

$$G^{total} = \sum_{i=1}^{N} n_i \left(\Delta G_{fi}{}^{o} + RT\ln y_i + RT\ln \widehat{\varphi}_i + RT\ln \frac{P}{P_0} \right) \quad (10)$$

Taking into consideration, the GFE of formation of solid carbon (C_s) species, the equation above can be modified as:

$$G^{total} = \sum_{i=1}^{N} n_i \left(\Delta G_{fi}{}^{o} + RT\ln y_i + RT\ln \widehat{\varphi}_i + RT\ln \frac{P}{P_0} \right) + n_c \Delta G_{fc(s)}{}^{o} \quad (11)$$

Minimization of equation (11) can be done in at least two ways. The more commonly employed procedure [11, 19] is the one which utilizes the concept of Lagrange's undetermined multipliers. This procedure requires the introduction of Lagrange variables in the equation (11) of the chemical potential of the system as disccued in detail by Abbot et al. [36]. The total expression of GFE with lagrange's multiplier can then be equated to zero. This gives rise to a system of N nonlinear equations which can be solved using any of the nonlinear equations solver routines. The resulting expression when Lagrange's multipliers are used is as follows:

$$\sum_{i=1}^{N} n_i \left(\Delta G_{fi}{}^{o} + RT\ln y_i + RT\ln \widehat{\varphi}_i + RT\ln \frac{P}{P_0} + \sum_k \lambda_k a_{ik} \right) = 0 \quad (12)$$

where λ_k is the Lagrange multiplier for element *k*.

In this work, we have employed a slightly different approach for GFE minimization. Rather than introducing the Lagrange's multipliers and solving the resulting nonlinear equations, we have minimized the expression (12) for GFE directly by using the constrained minimization '*fmincon'* routine in MATLAB®. This minimization yields the unknown mole fractions y_i for a given condition of n_i, *P*, and *T*.

Specie constraints are subjected to the mass balance for the different elemental species used in the system. For the case of CRM, CH_4, H_2O, O_2, CO, CO_2, H_2, and C(s) were taken as a reaction mixture. A selection of these compounds is very critical to the entire calculation as any wrong assumption or negligence of important component could give misleading results. Therefore, its choice should be made based on the experimental or industrial reformer data.

The mass balance constraints are:

$$\sum_i n_i a_{ik} = A_k \quad (13)$$

Here, a_{ik} is the number of atoms of the k^{th} element and, A_k is the total mass of the k^{th} element.

In this work, we have performed a detailed energy analysis of various case scenarios. This calculation is done by carrying out an energy balance across the CRM process using the following definition:

$$E_{in} = \sum n_{i,exit} H_{i,exit} - \sum n_{i,feed} H_{i,feed} \quad (14)$$

$n_{i,exit}$ is the number of moles of the component *i* in the exit stream and $n_{i,feed}$ is the number of moles of the component *i* in the entering stream.

Non-Ideality in the gas phase arises mainly in the high temperature and high pressure regimes, and most industrial reformers are known to operate in this condition. In particular, a typical SRM process is carried out at 900 ^{O}C and 20 bar [37]. Thus, in this work we have emphasized on more realistic scenarios whereby the non-ideality associated with the system is accounted for. In this regard, we have utilized fugacity coefficients to represent the concentration of the species involved in the reformer rather than the partial

pressures. The fugacity coefficients have been calculated using the RK, SRK and the PR EOS. Our findings showed that PR EOS was able to accurately predict the concentration profiles compared to the other EOS, and this can be attributed to its capability to model hydrocarbon and carbon dioxide mixtures quite accurately [12].

Fugacity Coefficient $\widehat{\varphi_i}$ calculation was carried out by using generic cubic EOS in the form of compressibility factor, z as follows:

$$z = \beta + (z+\in \beta)(z + \sigma\beta)\left(\frac{1+\beta-z}{q\beta}\right) \quad (15)$$

The fugacity coefficient is then calculated by substituting it in the following equation in terms of the compressibility factor:

$$\log(\widehat{\varphi_i}) = z - 1 - \log(z - \beta) - \frac{q \log\left(\frac{z+\sigma\beta}{z+\epsilon\beta}\right)}{\sigma-\epsilon} \quad (16)$$

Where;

$$q = \frac{a(T)}{bRT} \quad (17)$$

$$b = \Omega \frac{RT_c}{P_c} \quad (18)$$

$$a(T) = \Psi \frac{\alpha(T_r)\, R^2 T_C^2}{P_C} \quad (19)$$

$$\beta = \frac{bP}{RT} \quad (20)$$

The values and expressions of the different parameters used in the generic EOS are adopted from Abbot et al.[36] as shown in Table 1 on the next page.

Table 1 List of parameters used in the PR, RK and SRK EOS

Equation of state	$\boldsymbol{\alpha(T_r)}$	$\boldsymbol{\sigma}$	$\boldsymbol{\epsilon}$	$\boldsymbol{\Omega}$	$\boldsymbol{\Psi}$
RK	$T_r^{-1/2}$	1	0	0.08664	0.42748
SRK	$\alpha_{SRK}(T_r;\omega)$	1	0	0.08664	0.42748
PR	$\alpha_{PR}(T_r;\omega)$	$1+\sqrt{2}$	$1-\sqrt{2}$	0.07780	0.45724
$\boldsymbol{\alpha_{SRK}(T_r;\omega)}$	$\left[1+(0.480+1.574\omega-0.176\omega^2)\left(1-T_r^{1/2}\right)\right]^2$				
$\boldsymbol{\alpha_{PR}(T_r;\omega)}$	$\left[1+(0.37464+1.54226\omega-0.26992\omega^2)\left(1-T_r^{1/2}\right)\right]^2$				

Upon substitution of the parameters pertinent to each type of EOS, the generalized equation of state gets reduced to its original form.

To estimate the performance of the CRM process, we have considered percentage methane conversion, percentage carbon dioxide fixation, energy requirement and H_2: CO yield ratio as key indicator trends. These trends provide a clear guidance on the performance of the CRM process by providing inference about the effect of each operating scenario (T, P, and feed) on the performance of the system. This analysis not only helps in identifying optimized operating conditions but also helps in comparison of the different reformer technologies with the CRM process.

$$CH_4\%\ conversion = \frac{CH_{4,in\ feed} - CH_{4,in\ product}}{CH_{4,in\ feed}} \times 100 \quad (21)$$

$$CO_2\%\ conversion = \frac{CO_{2,in\ feed} - CO_{2,in\ product}}{CO_{2,in\ feed}} \times 100 \quad (22)$$

$$H_2O\ \%\ conversion = \frac{H_2O_{in\ feed} - H_2O_{in\ product}}{H_2O_{in\ feed}} \times 100 \quad (23)$$

The following procedure was employed in this study: Initially, equilibrium trends of the reaction mixture were studied as a function of temperature in the range of 200 ^oC to

1200 ^{o}C. Then, this examination was repeated for different pressures in the range of 1 to 20 bar, while keeping track of the energy requirement and the carbon deposition in each case scenario. Fugacity coefficients of the reaction mixture were calculated simultaneously using pertinent EOS. After this, the feed moles of the steam and oxygen were varied keeping carbon dioxide and methane fixed at 1 mole each. Steam was gradually added in the range of 0 to 1 mole, while that of oxygen was limited to 0.5 moles as more oxygen would lead to complete combustion of methane. This was done to maintain the reaction in line with stoichiometric ratios of the individual reforming processes. The main purpose of oxygen in the feed was to drive the energy intensive DRM and SRM processes in CRM, on the other hand, steam served as a source of hydrogen to maintain the syngas ratio (H_2/CO) more than 1. To capture the simultaneous effect of all the feed variations, three-dimensional visualization was intensively used.

3.2 Kinetic Calculations

In this chapter, calculation philosophy related to kinetics of a combined DRM/SRM reaction is discussed. The main aim of this work as mentioned previously is to develop a combined DRM/SRM kinetic model that could work similar to the conventional models available in the literature, more details about which are explained in section 5.2 (page 59). In the following section 3.2.1 on development of combined kinetic model, details about the development of a combined kinetic mechanism of the DRM/SRM process is explained and in section 3.2.2 (page 23), algorithm related to a pseudo-homogenous fixed bed reactor is explained.

3.2.1 Development of a Combined DRM/SRM Kinetic Model

Kinetic models are basically empirical correlations that are developed to understand the behavior of the system under certain conditions. Such analysis also helps in encapsulation of the experimental data in terms of mathematical model which shows interrelation between the different process variables. Kinetic models are also aimed in aiding simulation of complex reactors to portray and identify the important transport limitations of heat, mass, and momentum in a chemical reactor.

Previously in the literature, there were numerous studies that were targeted to develop complex kinetic models which describe the behavior of a single reforming process. In the present work, the Langmuir Hinshelwood Hougen Watson (LHHW) kinetic models by Xu et al. [30]and Verykios et al. [31] are used in a combined mode to simulate the behavior of a combined DRM/SRM system, the reactions which are involved in the combined DRM/SRM process are as follows:

$$r_{I,SRM} : CH_4 + H_2O \leftrightarrow CO + 3H_2 \quad (24)$$

$$r_{II,SRM} : CO + H_2O \leftrightarrow CO_2 + H_2 \quad (25)$$

$$r_{III,SRM} : CH_4 + 2H_2O \leftrightarrow CO_2 + 4H_2 \quad (26)$$

$$R_{CH_4,DRM} : CH_4 + CO_2 \leftrightarrow 2CO + 2H_2 \quad (27)$$

The rate expressions and the parameters that are used to model these reactions are adopted from the original work [30, 31] as follows :

Table 2 Kinetic rate expressions used in the combined DRM/SRM reaction

Rate Expressions	Kinetic Parameters
SRM Model by Xu et al.[30]	$k_1 = 2.636 \times 10^{13} \times e^{-\frac{28879}{T}} \frac{kmol.kPa^{0.5}}{kg.s}$
$r_{I,SRM} = \frac{k_1(P_{CH_4}P_{H_2O} - \frac{{P_{H_2}}^3 P_{CO}}{K_1})}{{P_{H_2}}^{2.5}(1+K_{CO}P_{CO}+K_{H_2}P_{H_2}+K_{CH_4}P_{CH_4}+\frac{K_{H_2O}P_{H_2O}}{P_{H_2}})^2}$ (28)	$k_2 = 1.219 \times 10^{11} \times e^{-\frac{8074.3}{T}} \frac{kmol}{kPa.kg.s}$
$r_{II,SRM} = \frac{k_2(P_{CO}P_{H_2O} - \frac{P_{H_2}P_{CO_2}}{K_2})}{P_{H_2}(1+K_{CO}P_{CO}+K_{H_2}P_{H_2}+K_{CH_4}P_{CH_4}+\frac{K_{H_2O}P_{H_2O}}{P_{H_2}})^2}$ (29)	$k_3 = 6.361 \times 10^{12} \times e^{-\frac{29336}{T}} \frac{kmol.kPa^{0.5}}{kg.s}$
$r_{III,SRM} = \frac{k_3(P_{CH_4}{P_{H_2O}}^2 - \frac{{P_{H_2}}^4 P_{CO_2}}{K_3})}{{P_{H_2}}^{3.5}(1+K_{CO}P_{CO}+K_{H_2}P_{H_2}+K_{CH_4}P_{CH_4}+\frac{K_{H_2O}P_{H_2O}}{P_{H_2}})^2}$ (30)	$K_{CH_4} = 6.65 \times 10^{-6} \times e^{\frac{4604.28}{T}} \frac{1}{kPa}$
	$K_{H_2O} = 1.77 \times 10^{3} \times e^{-\frac{10666.35}{T}} \frac{1}{kPa}$
	$K_{H_2} = 6.12 \times 10^{-11} \times e^{\frac{9971.13}{T}} \frac{1}{kPa}$
	$K_{CO} = 8.23 \times 10^{-7} \times e^{\frac{8497.71}{T}} \frac{1}{kPa}$
	$K_1 = 10266.76 \times e^{\frac{-2630}{T}+30.11} kPa^2$
	$K_2 = e^{\frac{4400}{T}-4.063}$
	$K_3 = K_1 \times K_2\ kPa^2$
DRM Model by Verykios et al.[31]	$K_1k_2 = 2.61 \times 10^{-3} \times e^{\frac{-4300}{T}} \frac{kmol}{kg.s.kPa}$
$R_{CH_4,DRM} = \frac{K_1k_2k_3k_4P_{CH_4}P_{CO_2}}{K_1k_2K_3P_{CH_4}P_{CO_2}+K_1k_2P_{CH_4}+K_3k_4P_{CO_2}}$ (31)	$K_3 = 5.17 \times 10^{-5} \times e^{\frac{8700}{T}} \frac{1}{kPa}$
	$k_4 = 5.35 \times 10^{-1} \times e^{-\frac{7500}{T}} \frac{kmol}{kg.s}$

Where,

$R_{CH_4,DRM}$: Rate of transformation of methane and carbon dioxide to carbon monoxide in a DRM reaction.

$r_{I,SRM}$: Rate of transformation of methane to carbon monoxide in an SRM reaction.

$r_{II,SRM}$: Rate of transformation of carbon monoxide to carbon dioxide in a water gas shift reaction (WGSR).

$r_{III,SRM}$: Rate of transformation of methane to carbon dioxide in an SRM reaction.

The Initial phase of the kinetic analysis was to validate the combined DRM/SRM model with the available results of the thermodynamic work. In order to accomplish this, only the kinetics of the proposed combined model was used in the mass conservation equations in the form of coupled ordinary differential equations as shown below:

Table 3 Coupled differential equations coded in MATLAB®

$\frac{dF_{CO}}{dW} = r_{I,SRM} - r_{II,SRM} + 2R_{CH_4,DRM}$	(32)
$\frac{dF_{H_2O}}{dW} = -(r_{I,SRM} + r_{II,SRM} + 2 \times r_{III,SRM})$	(33)
$\frac{dF_{CO_2}}{dW} = r_{II,SRM} + r_{III,SRM} - R_{CH_4,DRM}$	(34)
$\frac{dF_{H_2}}{dW} = 3r_{I,SRM} + r_{II,SRM} + 4r_{III,SRM} + 2R_{CH_4,DRM}$	(35)
$\frac{dF_{He}}{dW} = 0$	(36)
$\frac{dF_{CH_4}}{dW} = -(r_{I,SRM} + r_{III,SRM} + R_{CH_4,DRM})$	(37)

Here, molar flow rates $\left(\frac{mol}{h}\right)$ of each specie is denoted by 'F_i', it can be noted that the mass conservation equation of helium is taken as zero as it is an inert to the entire process. Helium is also used to pressurize the system if needed. Independent variable 'W' denotes catalyst weight in grams and 'r_i' $\left(\frac{mol}{g.h}\right)$ denotes the rates of each reaction of each specie.

Using the above mentioned coupled equations (32-37), the flow rates of each specie is obtained as a function of weight of the catalyst. The coupled ordinary differential equations are then solved over a range of catalyst weight until a steady flow of each component is obtained. For validation of the proposed combined model, the steady value of flow rate of each specie is compared with the thermodynamic results. Detailed results of this are mentioned in the section 5.2 (page 59).

3.2.2 Simulation of Pseudo-Homogeneous Fixed Bed Reactor

Initial design and scale up of any bench scale reactor requires understanding of many operational conditions related to the design and outcome of the scaled up reactor. In the beginning many alternative designs are suggested, however many of them are ruled out at certain stage of the progress of the project. The choice of the right reactor design is a very constrained decision related to both the economics and ergonomics of the process in addition to the competing market conditions. At this point, simulation of the alternative designs of the different suggested reactors becomes essential to get an understanding of the many challenges that can be anticipated for such a design.

Simulation of reactors are done at various scales, starting with the most basic and ending to the most complex which are very similar to the actual industrial reactors. In this

work, we have attempted to simulate a Pseudo-Homogeneous Fixed Bed Reactor, which is a basic category of the fixed bed class of reactor simulation. The aim of simulation of the reactor is to test the validity combined DRM/SRM model developed initially in this study.

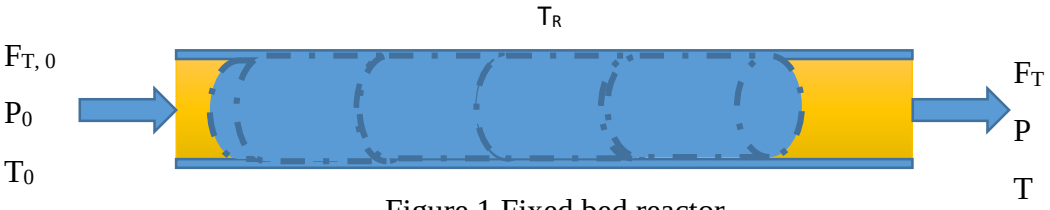

Figure 1 Fixed bed reactor

A basic pseudo homogenous fixed bed reactor is based on the assumption that the concentration and temperature gradient occurs only in the axial direction while neglecting radial gradients. The reactor is also assumed to be cylindrical in dimension as shown in Figure 1. Overall flow of the fluid through the reactor is considered to be plug flow in nature, which serves to be the only transport mechanism.

For a fixed bed reactor, with a catalyst bed density of ρ_B with specie i in the reaction mixture, the following mass conservation equation is applied (adopted from Froment et al.[30]):

$$\frac{d(F_i)}{dz} = r_i \times \rho_B \times A_t \qquad (38)$$

Upon applying this, the coupled ordinary differential equation for all the species become as shown below in Table 4 :

Table 4 Coupled mass conservation ordinary differential equations

$$\frac{dF_{CO}}{dz} = (r_{I,SRM} - r_{II,SRM} + 2R_{CH_4,DRM}) \times \rho_B \times A_t \quad (39)$$

$$\frac{dF_{H_2O}}{dz} = -(r_{I,SRM} + r_{II,SRM} + 2 \times r_{III,SRM}) \times \rho_B \times A_t \quad (40)$$

$$\frac{dF_{CO_2}}{dz} = (r_{II,SRM} + r_{III,SRM} - R_{CH_4,DRM}) \times \rho_B \times A_t \quad (41)$$

$$\frac{dF_{H_2}}{dz} = (3r_{I,SRM} + r_{II,SRM} + 4r_{III,SRM} + 2R_{CH_4,DRM}) \quad (42)$$

$$\frac{dF_{He}}{dz} = 0 \quad (43)$$

$$\frac{dF_{CH_4}}{dz} = -(r_{I,SRM} + r_{III,SRM} + R_{CH_4,DRM}) \times \rho_B \times A_t \quad (44)$$

The following equation (adopted from Fogler et al.[38]) is used as energy balance equation to find the temperature profile across the bed:

$$\frac{dT}{dz} = \frac{\frac{Ua(T_a - T)}{\rho_B} + \sum \Delta H_{rxn,j} r_j}{\sum F_i C_{p_i}} \times \rho_B \times A_t \quad (45)$$

Where,

$U = overall\ heat\ transfer\ coefficient\ \left(\frac{J}{hr.m^2K}\right)$

$T_a = Outer\ wall\ temperature\ (K)$

$A_t = crossectional\ area\ of\ the\ reactor\ (m^2)$

$C_{p_i} = heat\ capacity\ at\ constant\ temperature\ of\ specie\ i$

$\Delta H_{rxn,j} = enthalpy\ of\ reaction\ j$

For the purpose of momentum balance, the following equation proposed by Ergun et al.[39] is used:

$$\frac{dP}{dz} = -\frac{G}{\rho_g D_p}\left(\frac{1-\varphi}{\varphi^3}\right)\left[\frac{150(1-\varphi)\mu_{mix}}{D_p} + 1.75G\right] \quad (46)$$

Where,

$\rho_g = gas\ density\ \left(\frac{g}{m^3}\right)$

$D_p = particle\ diameter\ (m)$

$\varphi = porosity\ of\ the\ catalyst$

$\mu_{mix} = viscosity\ of\ gas\ mixture$

$G = superficial\ mass\ velocity\ (\frac{g}{m^2.hr})$

Equations (39-44) needs to be coupled together and solved in an ordinary differential equation solver. In this study, '*ode15s'*, ordinary differential equation solver was used as the equations were forming a *'stiff'* system.

As can be noted from equations (39-44), the independent variable is z, which represents the length of the reactor. The initial conditions that were defined to solve the coupled ordinary differential equation (39-44) are the following:

At $z = 0$,

$F_i = F_{i,0}\ (Feed\ molar\ flow\ rate)$

$T = T_g\ (Feed\ temperature\ of\ the\ gas)$

$P = P_0, Feed\ pressure\ of\ the\ reformer\ gas$

Results are then obtained at various feed conditions to analyze different case scenarios for understanding the behavior of the system and also to test the proposed combined kinetic model against the thermodynamic results obtained in earlier in this study.

The important pieces of information that could be derived from such a reactor bed simulation after preliminary testing of the kinetics are the following:

1) Inference on the reactor bed length that is needed to achieve a certain conversion.
2) Tube diameter needed to reduce the pressure drop.
3) The wall temperature that needs to be kept to keep up the reactor temperature to maintain certain conversion level.

CHAPTER IV

MODEL VALIDATION

4.1 Validation of Equilibrium Results

As mentioned earlier, CRM is a relatively new process compared to the conventional SRM, DRM and POX processes. Extensive literature focusing on the various aspects (including thermodynamics, kinetics and reactors) of these processes is available. In contrast to earlier studies, which have employed well-established commercial software packages like Aspen plus®[18, 20], an elaborate programmed was developed in this study in Matlab®. In this process, we used a built-in minimization tool *'fmincon'* which directly minimizes the GFE of the system without any introduction of Lagrange undetermined multiplier unlike few of the studies [11, 13, 36] reported in the literature. Therefore, before proceeding further and in order to verify the accuracy of the proposed model results, sufficient attempts were made to validate the proposed model against the previously published experiments as well as theoretical models.

Due to unavailability of published experimental reports on the CRM process (for the conditions under current analysis), we have used the currently accessible DRM experimental results to validate our model.

A Comparison of the proposed model results with the previously published experimental DRM results by Khalesi et al. [40] and Liu et al. [41] in terms of the CH_4 percentage conversion is shown in

Figure 2. Their results were found to be in a good agreement with this model specifically in the high temperature regimes, typically in the temperature range of 700 ^{o}C

and above. As DRM is a highly endothermic process, it requires high temperatures to bring the process to a feasible regime where in positive CH_4 and CO_2 conversions could be achieved, this is also evident from the experimental results shown in Figure 2.

The reaction temperature is observed to be a controlling factor leading to kinetic limitations, as can be seen, at lower temperatures the conversion approach to equilibrium is much less compared to higher temperatures which indicates that the process is kinetically limited, which is also claimed by Cui e al's proposition [42]. Reactant conversions are seen to be increasing with the increase in temperature. In particular, temperatures above 700 ^{o}C is seen to be a favorable regime for CH_4 to CO conversions. The CH_4 % conversion profile for strontium based catalyst is seen to incline more towards equilibrium conversion profile owing to high activity of the catalyst under such conditions, however in general; kinetic limitations are always seen to effect at lower temperatures typically below ~500 ^{o}C. High agreement of the proposed model with the results reported by Khalesi et al.[40] over a wider range of temperature (500 ^{o}C to 850 ^{o}C) shows good validity of the model.

The carbon deposition trends reported in our previous study by Noureldin et al.[11], as shown in Figure 3 were also found to be in an excellent agreement with our model results. Subsequent to this validation study, it is quite clear that the equilibrium analysis carried out using our technique holds credibility so as to provide better understanding of a reformer system.

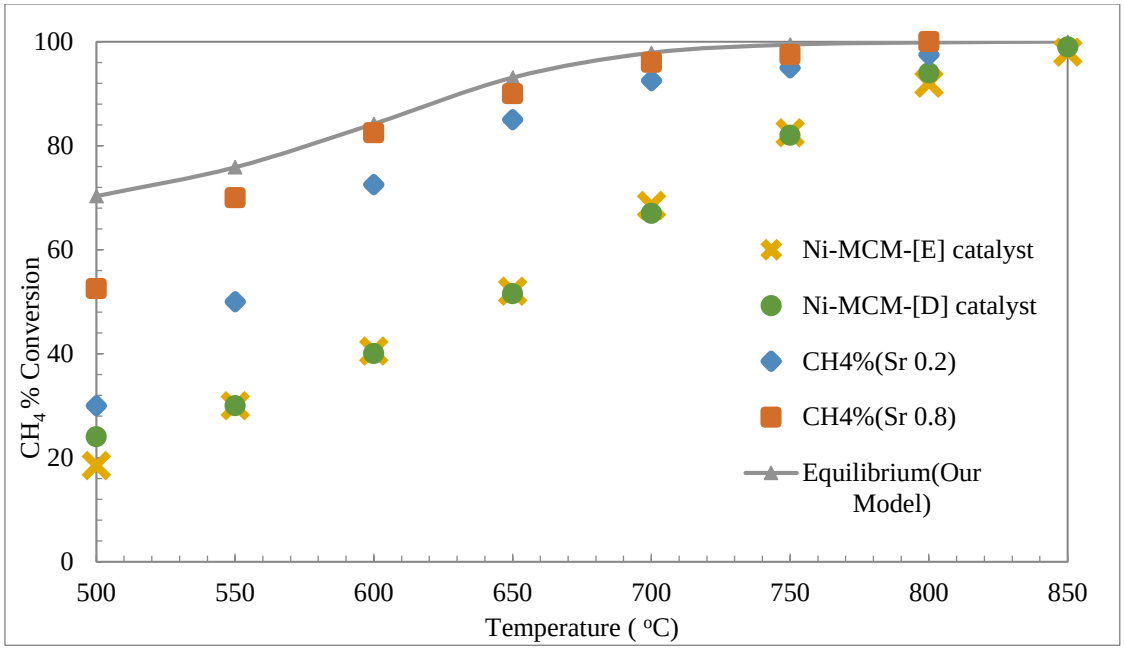

Figure 2 Model validation with experimental results reported by Khalesi et al. [38] and Liu et al. [39]

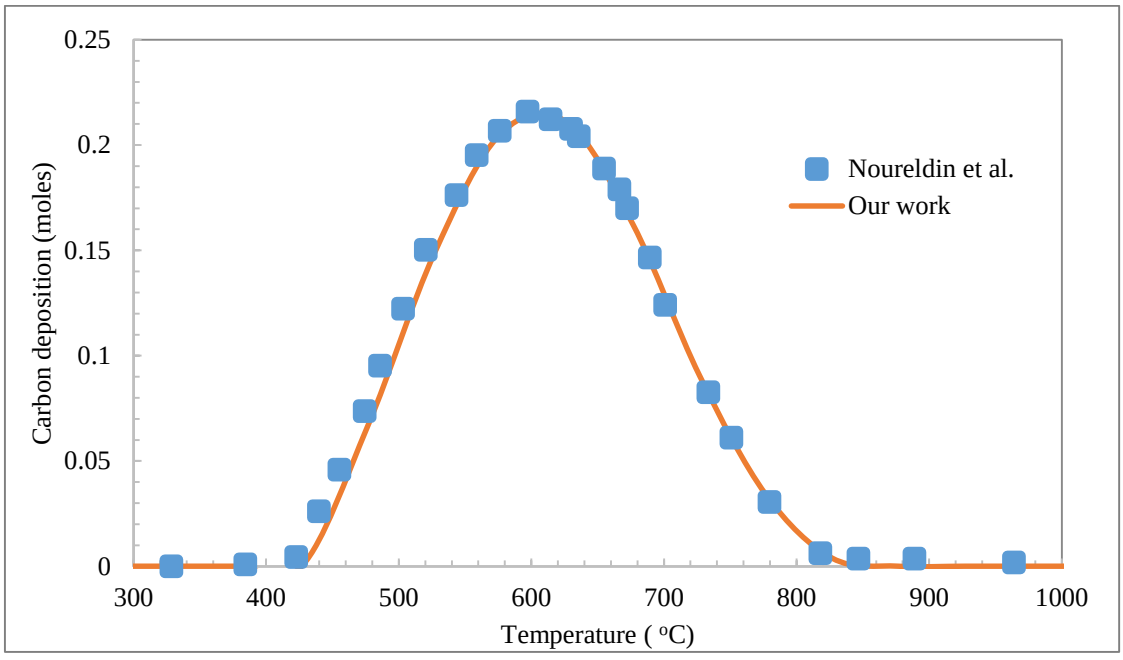

Figure 3 Model validation with simulation results reported by Noureldin et al. [11]

4.2 Validation of Kinetic Results

Previously in the literature, there were reported many kinetic models on the individual steam reforming and dry reforming reaction [32-35]. And it has also been consistently reported in the literature regarding the added benefits of operating the reformer in a combined mode. Except for thermodynamics, there are very limited data points available that explain the kinetics behavior of such complicated combined system. As mention earlier, significant efforts were made in this study to understand the combined characteristics of reforming system, for which attempts were made to see the effect of the combined model predictions of the conventional individual reforming models. So as an initial finding of this study, the focus was diverted to validate the combined DRM/SRM kinetic model with thermodynamic equilibrium predictions. Figure 4 shows the calculated CO and H_2 moles using both thermodynamic and kinetic analysis. As can be noted, both the trends are seen to be in good agreement with each other over a considerable range of temperature (900K to 1500K).

At a lower temperature range of 500K to 900 K, hydrogen trend deviates by a small extent from the equilibrium values, this is expected to be addressed by tuning the kinetic parameters, which in this study were adopted from the original studies without any pre fitting. The proposed combined model was also tested over a range of pressure (Figure 5) and again, a very good agreement was found between the kinetically and thermodynamically calculated results. From Figure 4 and 5, it can be noted that the thermodynamic and kinetic trend agree considerably well throughout the temperature and

pressure range, which shows that the proposed combined model holds credibility in predicting the product distribution of the combined DRM/SRM process.

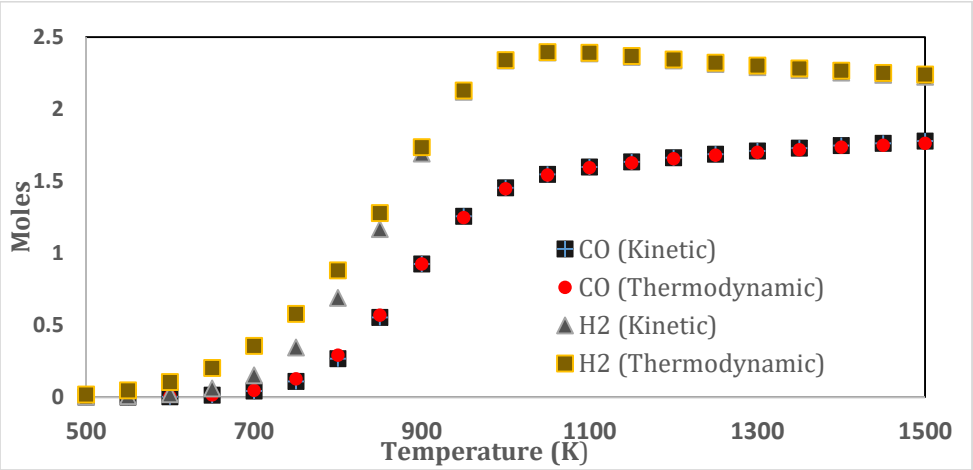

Figure 4 Kinetic Vs Thermodynamic trends of CO & H_2 for DRM/SRM combined reforming

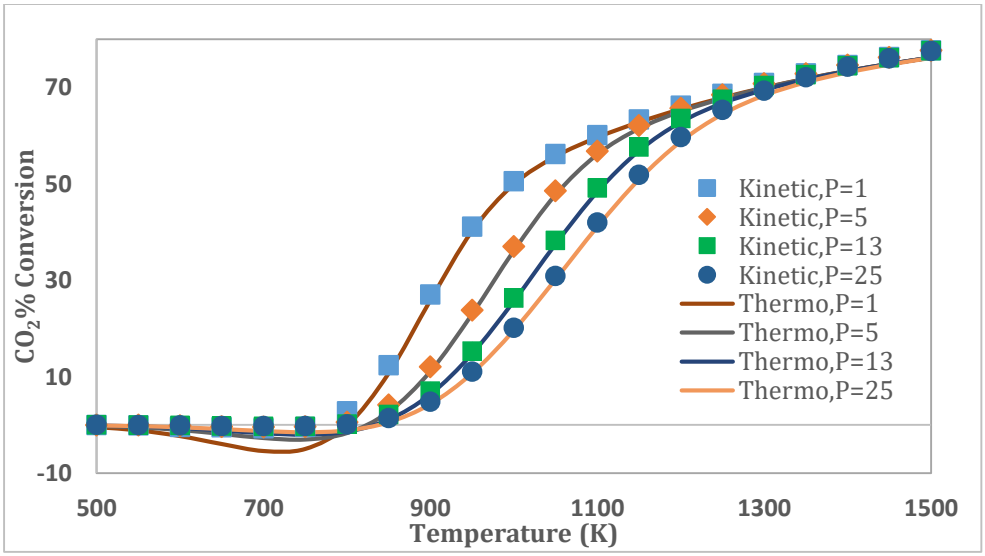

Figure 5 Comparison of kinetic and thermodynamic % CO_2 conversion up to 25 bar of pressure

CHAPTER V

RESULTS AND DISCUSSION

In this chapter, all the results obtained in this study are discussed. In the first sub section 5.1 on thermodynamic analysis, explanations about the various process parameters that control the reforming reaction are explained. This section also explains the effect of non ideality that arise at high pressure operation of the reformer. In the next section 5.2 on kinetic analysis (page 59), detail discussion on the kinetics of the combined DRM/SRM model is explained.

5.1 Thermodynamic Analysis

5.1.1 Non Ideality of Reforming Mixture

Except for the low pressure and high temperature conditions, the reaction mixture of a reformer is expected to behave non-ideally at all other conditions [36, 43]. This non-ideality is mostly attributed to the differences between the physico-chemical properties of the individual reacting species at respective process condition. Essentially, most of the gaseous mixtures behave non-ideally at pressure and temperature ranges in which the reformers typically operate (900 ^{o}C and 20 bar) [37]. In this work, non-ideality is accounted for by incorporating mixture fugacity coefficient in the GFE equation (11) as described in the methodology (page 12).

In Figure 6, a comparison between the calculated fugacity coefficients using the RK, SRK and PR EOS is shown. From this figure, it can be seen that, while there is a significant deviation from the ideality of the mixture at higher and lower temperatures as predicted by the three EOS; however, the SRK EOS is found to deviate consistently from

the results of PR and RK EOS throughout the temperature range of 200 ºC to 1200 ºC . The reason for this is attributed to the fact that SRK EOS is good at representing only the hydrocarbons, while the reaction mixture considered in this system includes non hydrocarbon gases as well (CO_2, H_2O, CO and H_2) [44].

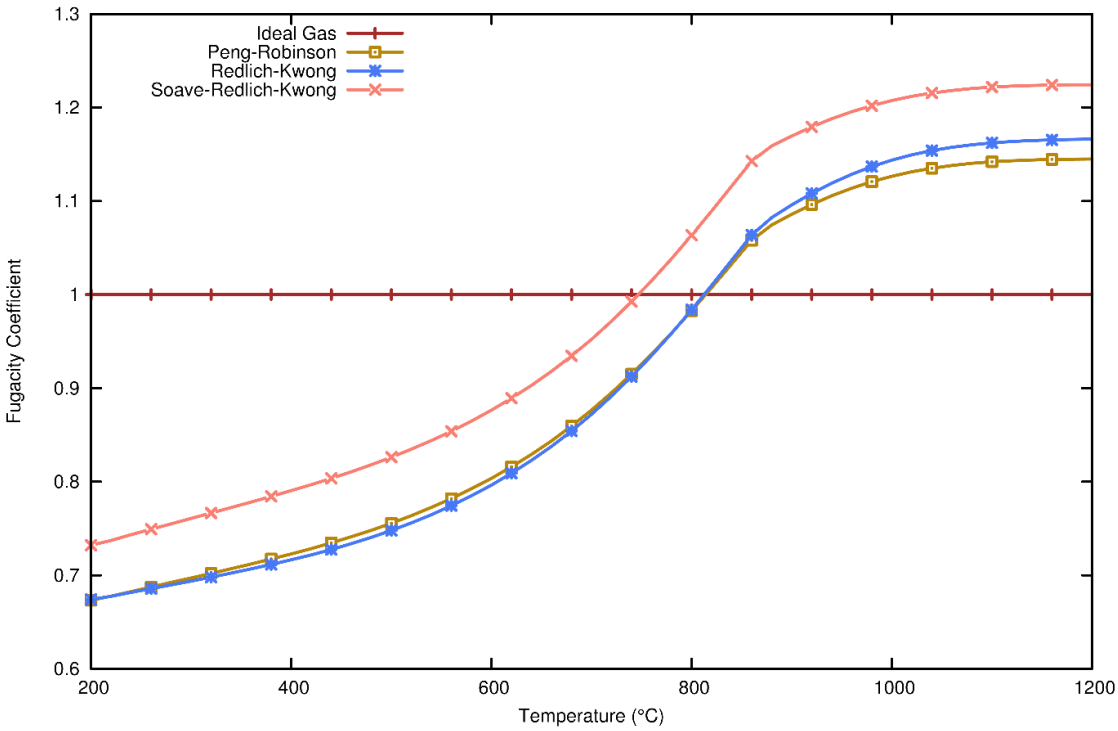

Figure 6 Fugacity coefficient trends of the reaction mixture at 20 bar using PR, RK & SRK EOS.

Although, the performance trend exhibited by PR EOS is very similar to the one displayed by SRK EOS, the latter is generally superior in calculation of both the liquid and gaseous densities of mixture of of hydrocarbon, water, air and combustion gasses,

which represents the typical reformer reaction mixture [12, 43]. On the otherhand, even though the results generated from the RK EOS closely agree with those from PR EOS, RK EOS displays poor performance in representing vapor-liquid mixture behaviours above a ratio of 0.5 T/T_c. Thus at lower temperature's, RK EOS may not be able to provide accurate results comparitively [45]. For these reasons, to be more flexible, PR EOS has been used in all the subsequent calculations reported in this study.

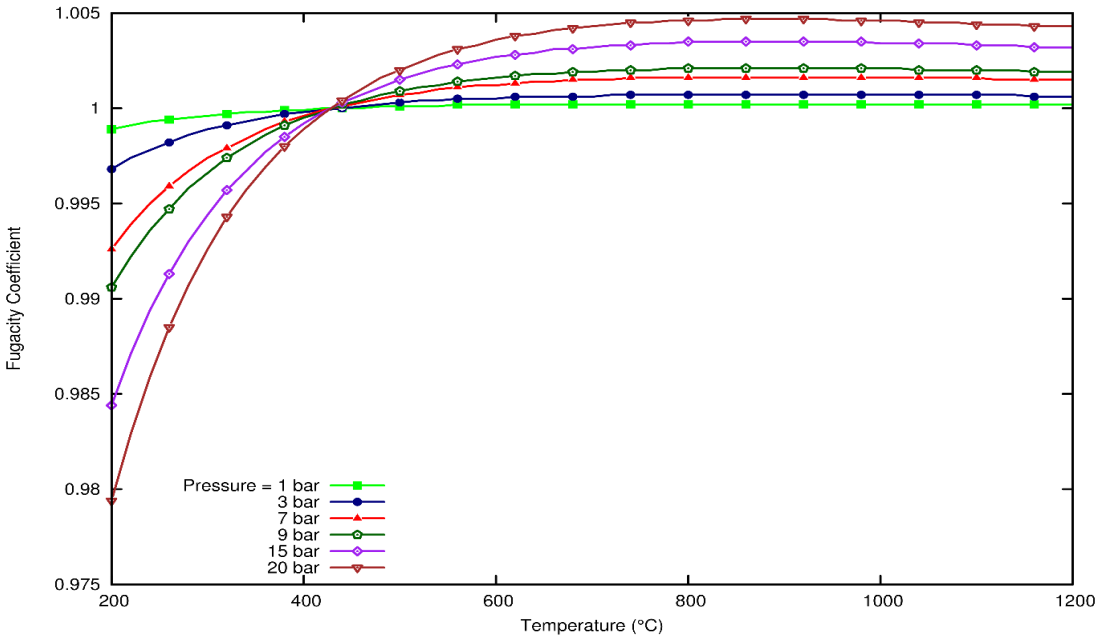

Figure 7 Fugacity coefficient trends of carbon dioxide using PR EOS

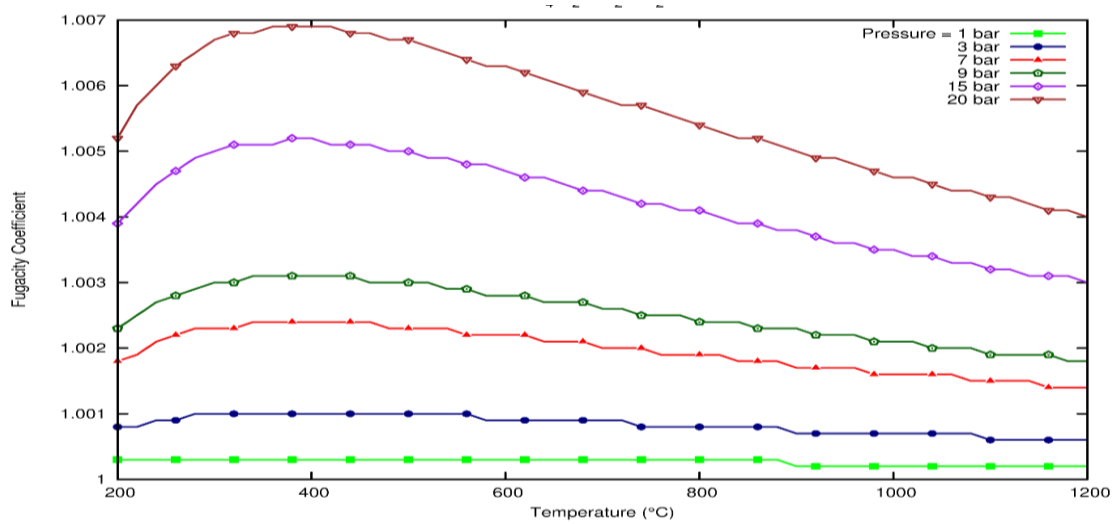

Figure 8 Fugacity coefficient trends of carbon monoxide using PR EOS

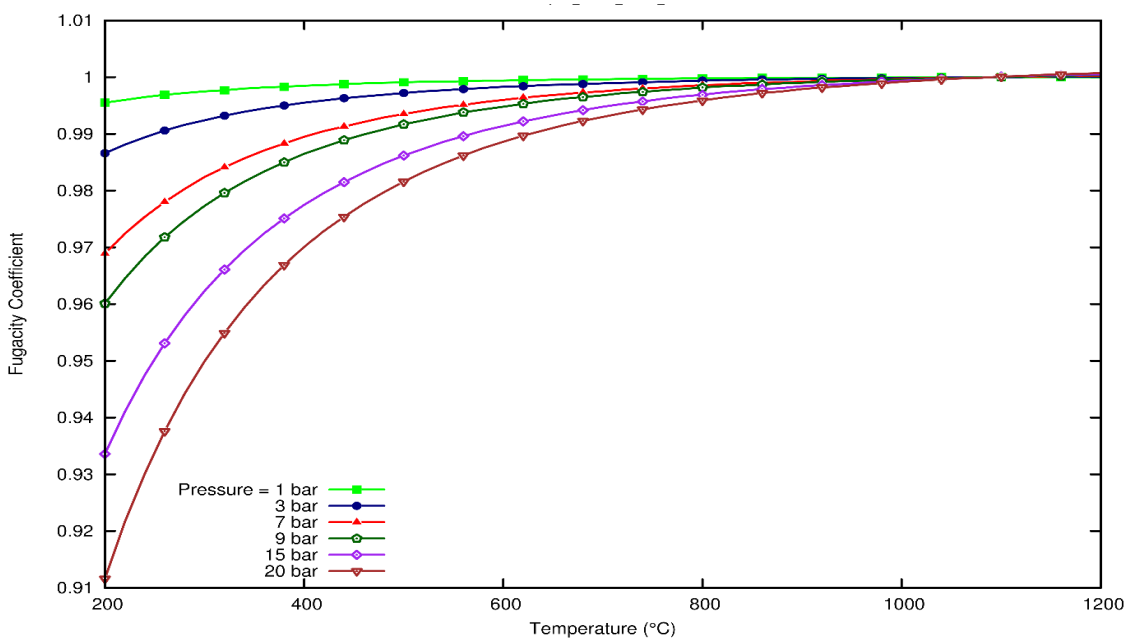

Figure 9 Fugacity coefficient trends of steam using PR EOS

In order to understand the non-ideality associated with the system, individual specie fugacity coefficients were calculated using PR EOS. Figure 7-9 show the individual fugacity coefficient trends of carbon monoxide, carbon dioxide and steam as a function of temperature and pressure. The main reason behind this was to quantify the effect that these compounds have at high temperature and pressure conditions. It can be observed that all the species behave very differently at the same conditions. Significant deviation from ideality was observed at high pressures at which typically most of the industrial reformers operate. It is to be noted that the individual plots show the behavior of these species when they are not in the combined mode, in a reaction medium these compounds behave very differently and their interaction with the other compounds also influence these deviations. So to work around this, combined fugacity coefficient was calculated which cumulates the effect of all the deviations. Figure 10 shows the calculated fugacity coefficient of the reformer inlet gas mixture using the PR EOS. It was observed that the fugacity coefficient of the gaseous mixture approaches unity when the temperature reaches ~800 ^{o}C for all studied pressure conditions. Deviation from ideality for feed mixture can clearly be seen when the temperature goes above ~800 ^{o}C (increased fugacity coefficient) as well as when the temperature is below ~800 ^{o}C (decreased fugacity coefficient). This is a general observation in case of all studied pressure conditions, except for 1 bar condition. For typical industrial operating condition (of 900 ^{o}C and 20 bar), the reaction mixture is expected to deviate by approximately +10% from ideality. This indicates that the consideration for the non-ideality of the reaction mixture becomes indispensable at any condition other than a temperature of ~800 ^{o}C and a pressure greater than 1 bar.

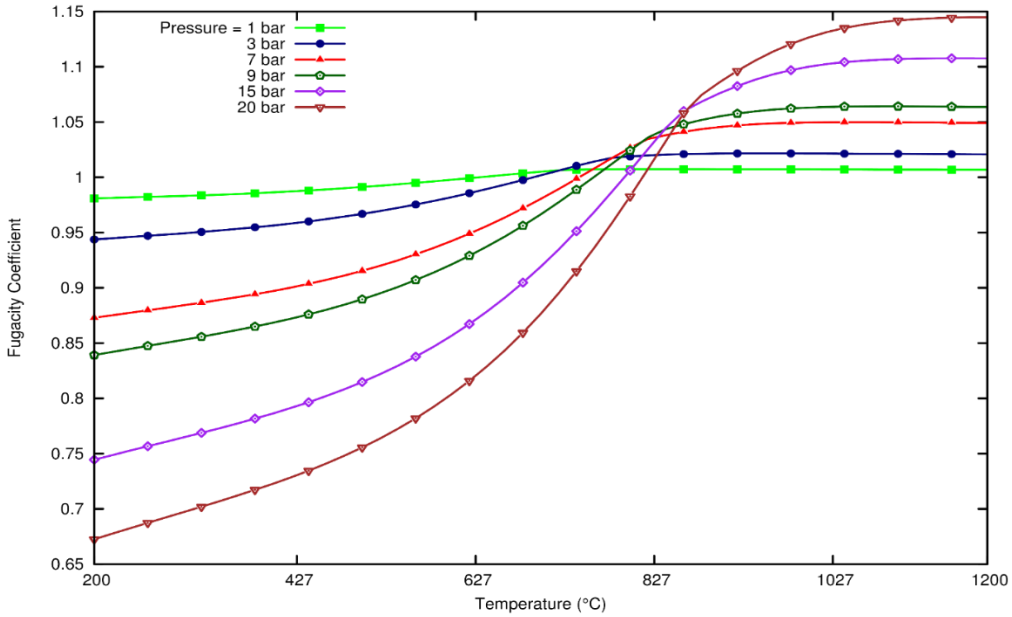

Figure 10 Fugacity coefficient of the inlet mixture at various pressures calculated using the PR EOS.

The analysis mentioned above demonstrates that non-ideality is one of the most critical factors to affect the equilibrium state of the reforming mixture. In particular, high pressure operation of the reformer is more impacted by the non-ideal behavior of the system. Therefore, it becomes sufficiently evident that any reliable thermodynamic analysis of reforming process at near industrial conditions needs to properly incorporate non-ideality in the simulations.

5.1.2 Equilibrium Temperature Effect

In the previous section, the effect of non-ideality on the thermodynamic equilibrium calculations of a reformer mixture is studied. Here, we have looked at the effect of temperature at which the reforming reaction takes place. At each temperature point, we calculated the equilibrium product distribution and evaluated it in terms of the CH_4 as well

as CO_2 percentage conversions, H_2 : CO yield ratio, amount of solid carbon deposited and also the amount of energy required to sustain this reaction.

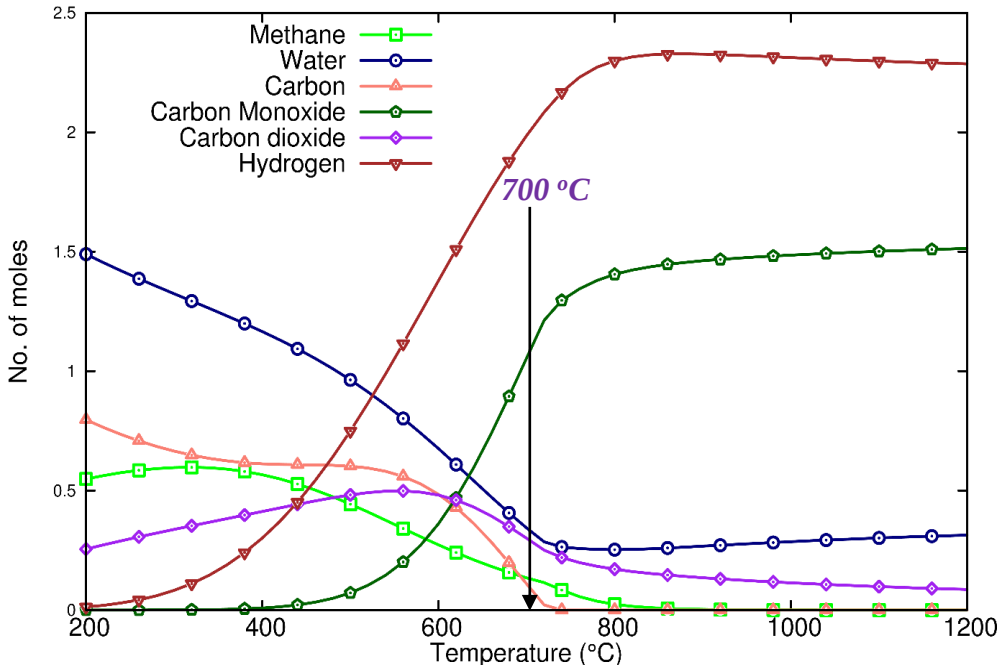

Figure 11 Equilibrium product distribution of the reforming mixture

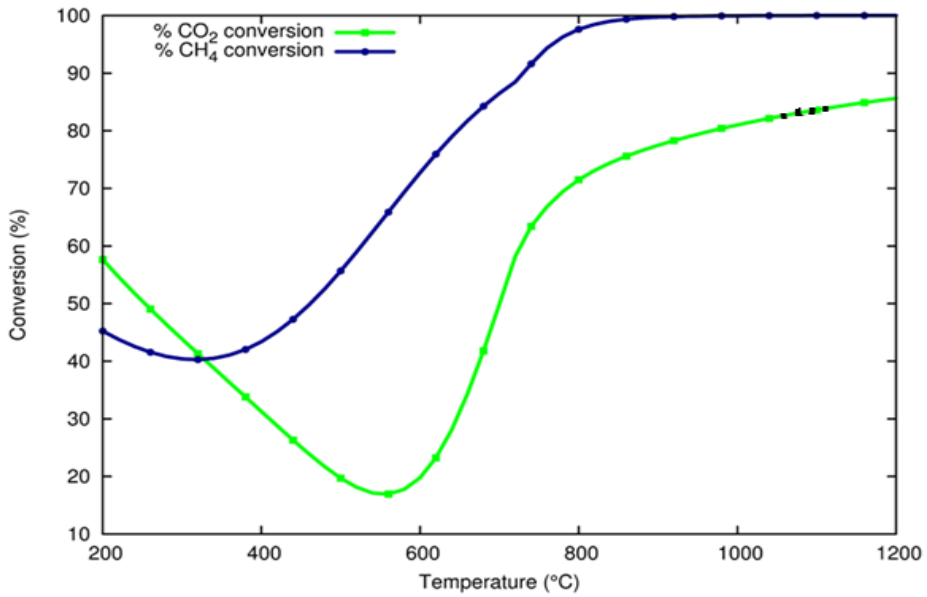

Figure 12 Percentage CO_2 and CH_4 conversions of the reforming mixture

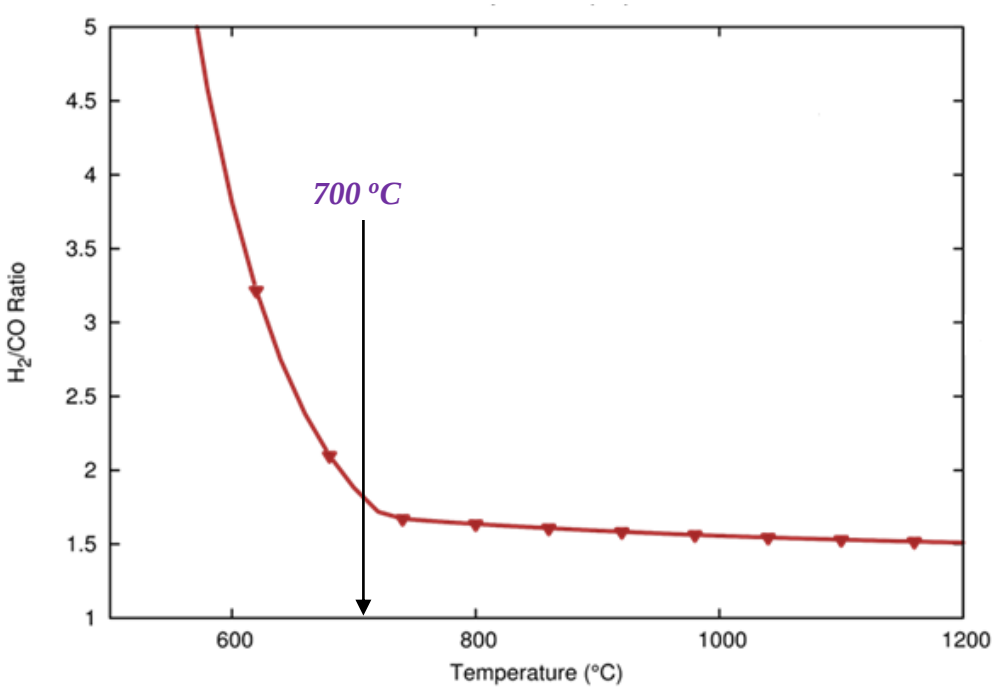

Figure 13 H_2: CO yield ratio of the reforming mixture

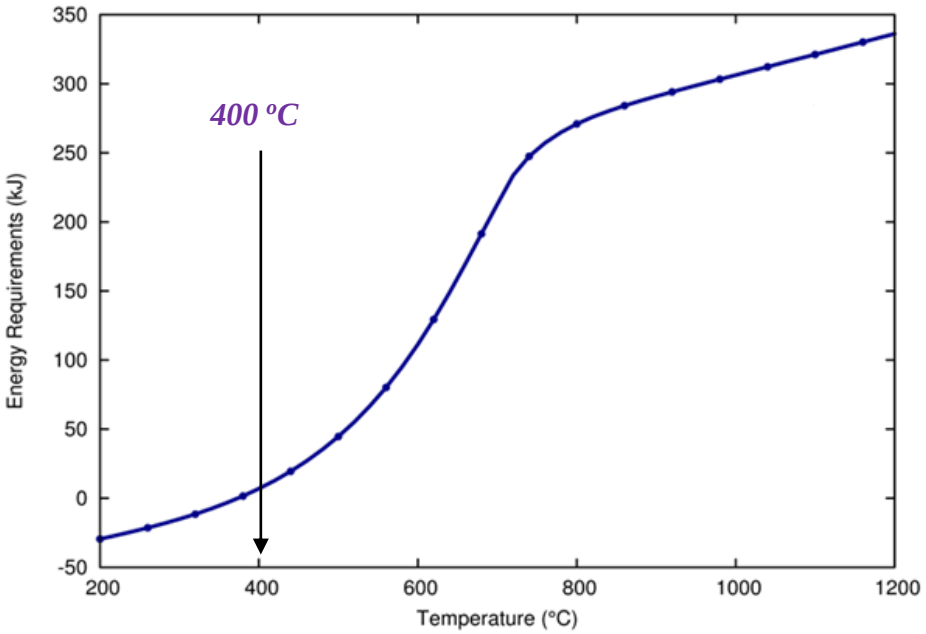

Figure 14 Energy requirements of the combined reforming process over a range of temperatures from 200 °C to 1200 °C at a pressure of 1 bar

Reforming reactions are highly temperature sensitive. The chemical potential of a compound and in turn it's GFE of formation is a function of temperature. For a typical CRM process at a feed mole ratio of CH_4:H_2O:O_2:CO_2 = 1:0.6:0.1:0.6, Figure 12-14 illustrates the various performance evaluation trends as a function of temperature at 1 bar pressure. For this feed ratio, it was observed that the reaction behaves auto thermally at ~ 400 °C temperature at 1 bar pressure (Figure 14). A closer analysis of Figure 14 leads to the finding that at a temperature of ~700 °C, the syngas (H_2:CO) yield ratio is ~2:1 . Depending on the application of syngas, H_2:CO ratio might be of prominence. For instance, a syngas ratio of 2:1 is imperative if it is to be used in a cobalt catalyst based FTS process [46]. At this condition, ~50 % CO_2 and ~85 % CH_4 conversions are observed. An amount of ~200 kJ is required to sustain this process, and ~0.25 moles of solid carbon

is deposited. With a slight increase in the temperature by 20-30 °C, carbon deposition reduces to a negligible amount. But, this presents a trade off as energy demand increases by 20 kJ along with an offset of H_2:CO ratio of ~1.5 with a significant increase in feed conversion. This analysis helps in finding an optimized condition at which we could operate a typical CRM process to maintain a syngas (H_2:CO) ratio near to 2.

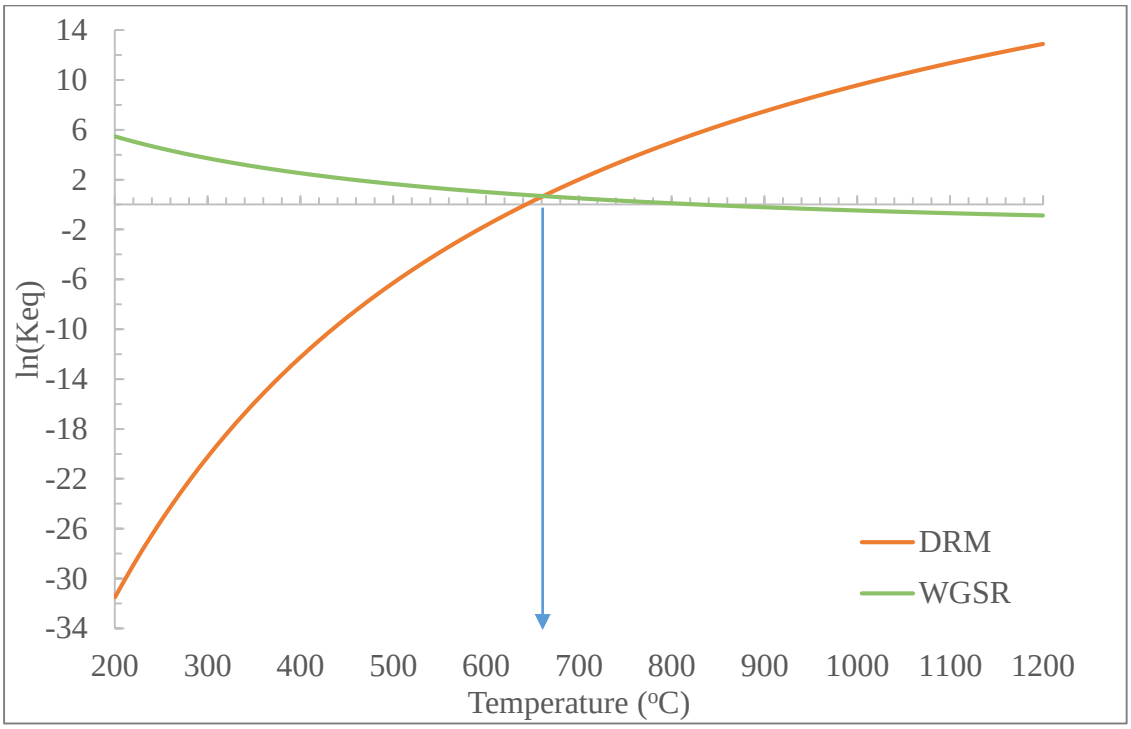

Figure 15 An illustration of the competition between the WGSR and DRM as a function of temperature.

The CH_4 % conversion (Figure 12) under CRM process follows similar trends to the SRM and DRM reported by Noureldin et al. [11]. The carbon deposition trend in Figure 11 indicates significant carbon formation below ~700 °C which agrees with the

SRM and DRM results reported by Noureldin et al.[11]. The presence of three oxidants (CO_2, H_2O, and O_2) in CRM process reduces carbon deposition significantly as compared to individual SRM, DRM and POX process reported by Noureldin et al. [11]. This highlights the benefit of CRM process over individual reforming technologies. CO_2 % conversion (Figure 12) however, suffers from a reduced conversion compared to DRM process, which can again be attributed to the presence of three oxidants. As seen from Figure 12, the CO_2 % conversion increases quite steadily after 600 °C, which indicates that reverse water gas shift reaction (RWGSR) (Equation 25) accompanies the DRM reaction (as a part of CRM) at any temperature above ~ 600 °C. In Figure 15 it can be seen that the WGSR reaction rates are lower than that of DRM reaction above ~600 °C. This suggests that the CRM process should be carried out at temperatures above 600 °C to get a net CO_2 % conversion increase.

The aforementioned results indicate that temperature is a very critical parameter for the optimization of the CRM, which affects not only the energy requirements but also other important product distribution. In particular, we can observe that a temperature of ~700 °C is reasonable for the operation of a CRM process which would serve a syngas yield ratio of ~2:1 while keeping carbon deposition negligible. This temperature also provides a reasonable CO_2 % conversion of ~50% while keeping energy requirement below 200 kJ.

5.1.3 Equilibrium Pressure Effect

As a part of equilibrium thermodynamic analysis of the CRM process, in the previous section a very close analysis of the independent effects of temperature on the

equilibrium product distribution was carried out. In this section, we have evaluated the effect of pressure along with temperature on a CRM process by observing various performance evaluation trends including the percentage CH_4 & CO_2 conversions, carbon deposition, the syngas yield ratio and the corresponding energy requirements.

The GFE is a logarithmic function of pressure. Thermodynamically, a change in pressure changes GFE of the system and pushes it in the reaction coordinates in which the effect is minimized. The effects due to the variation of pressure are shown in Figure 16-20. As pressure increases, we observe a steady decrease in methane conversion over the complete temperature range. As discussed in section 5.1.2 Equilibrium Temperature Effect, a decreasing trend up to 400 °C and then an increasing tendency in methane conversion is seen. A maximum CO_2 conversion of 85% is realized at a very high temperatures for this combination of input feed molar ratios. A reversal of trend is observed in CO_2 % conversion as a function of pressure. A minor increase in CO_2 % conversion up to 600 °C followed by a significant decrease as a function of pressure is observed.

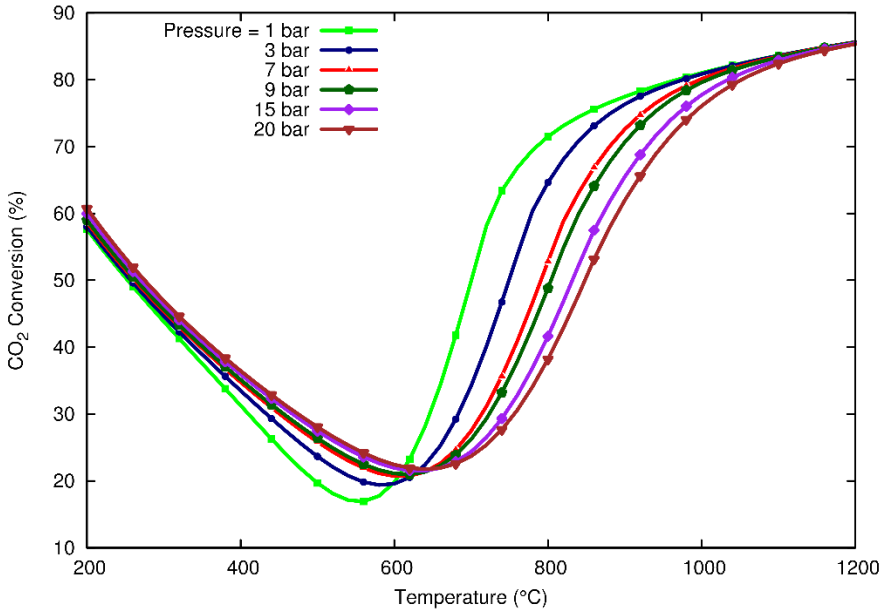

Figure 16 Methane % conversion as function of temperature

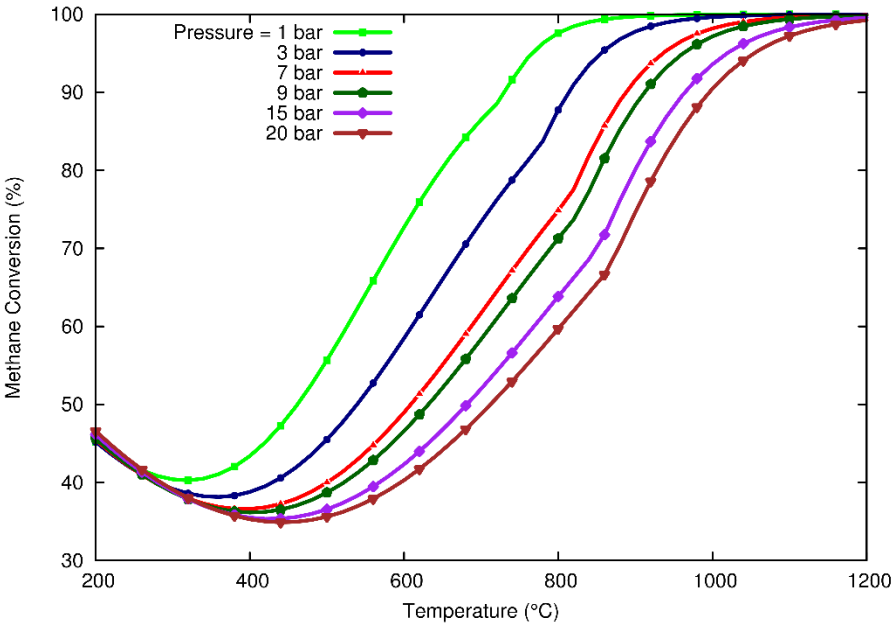

Figure 17 Carbon dioxide % conversion as function of temperature

A similar reversal of trends is also seen in carbon deposition (Figure 18). At low temperature, it decreases as pressure increases and at temperatures higher than 600 °C, a significant increase with pressure is observed in carbon deposition. Syngas yield ratio as shown in Figure 19 increases with pressure up to 800 °C and then slightly decreases to reach a steady value of 1.5.

Energy requirements shown in Figure 20 are noted to decrease throughout the range of pressure examined in this study. However, the reaction remains slightly exothermic at lower temperatures up to ~400 °C, and thereafter endothermicity increases steadily with an increase in temperature.

This analysis leads to the inference that temperatures higher than ~850 °C at low pressures result in no considerable incentive in terms of either syngas quality or conversions, but at the same time requires higher energy cost.

Thus, a temperature of ~800 °C and 1 bar seems to be an optimum for a feed ratio of CH_4:H_2O:O_2:CO_2 = 1:0.6:0.1:0.6 operating at an energy requirement of 275 kJ yielding a syngas ratio of 1.5.

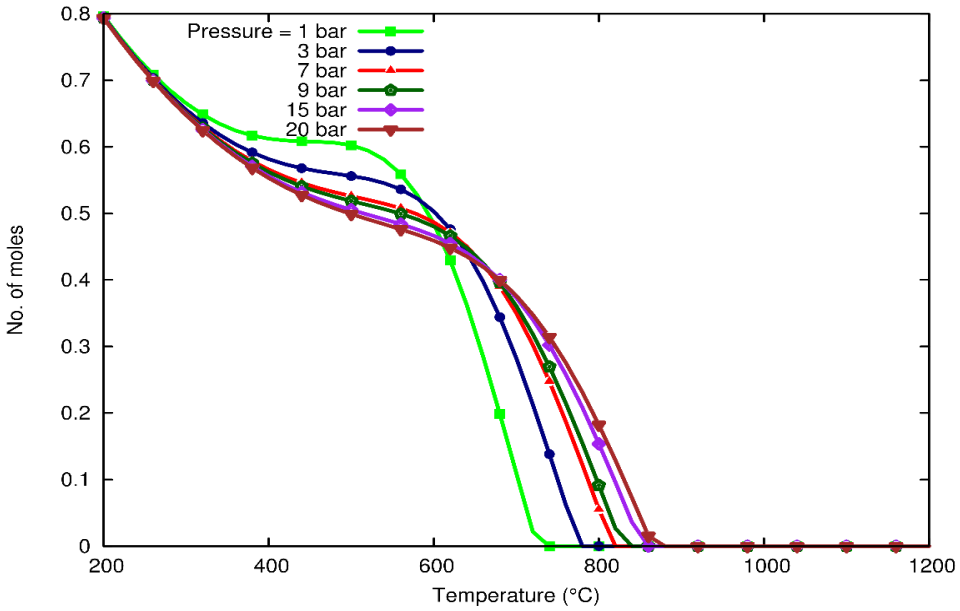

Figure 18 Carbon deposition as function of temperature

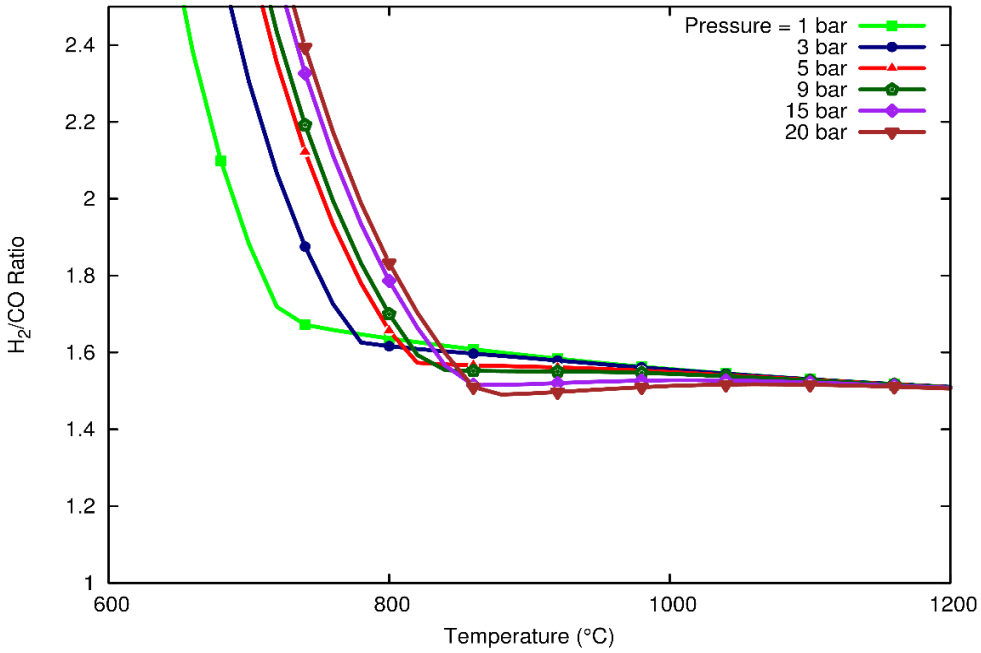

Figure 19 H_2: CO syngas yield ratio

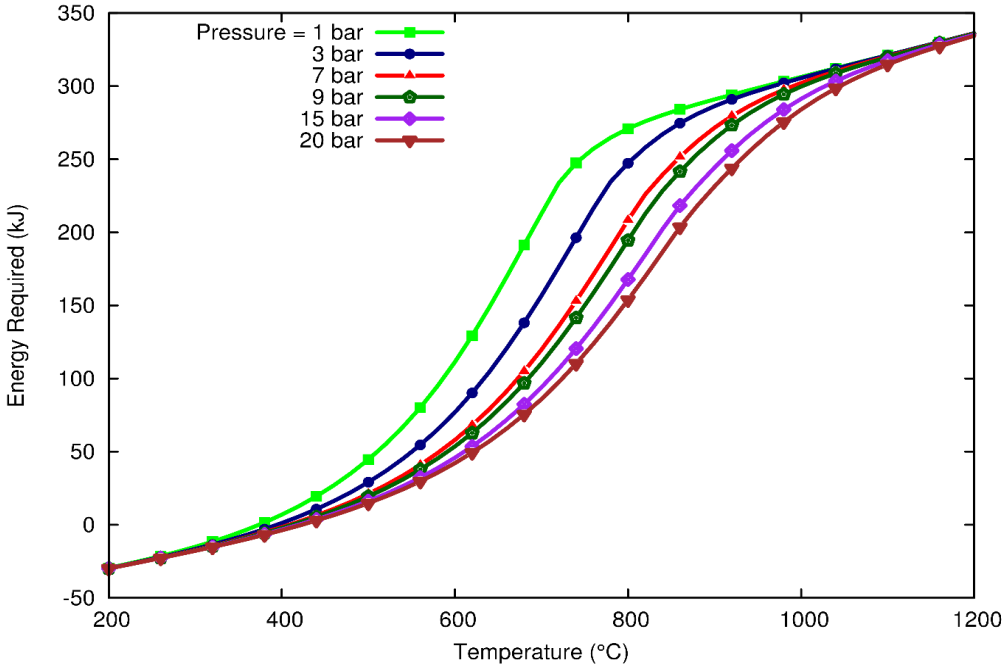

Figure 20 Effect of pressure on energy requirements.

5.1.4 Effect of Steam on Dry Reforming Reaction

DRM reactions typically produce syngas (H_2: CO) yield ratio of 1:1. Though, this ratio is good for producing long chain hydrocarbons as mentioned previously, but there are only few catalyst which can work on such a low ratio in an FT process and the integration of a DRM reactor with existing infrastructre (which typically in many cases work at higher syngas yield ratio) might present many other challenges. In view of this, there are many process limitations that can be solved when DRM can be conducted in a more hydrogen rich environment. As mentioned previously in chapter 1 (page 1), to increase the syngas ratio, the DRM process can be carried out in the presence of steam. Addition of steam increases the hydrogen content of syngas to raise its H_2:CO ratio to 2:1 and above based on the amount of amount steam fed to the reformer. High steam content

also enables lesser carbon deposition on the catalyst surface and thus serves dual advantages of improved syngas yield ratio and reduced carbon deposition.

Figure 21 shows the various reformer performance trends that are influnced by the addition of steam to the DRM process. As is evident from

Figure 21 (a), methane conversion decreases with increasing amount of steam in the system at lower temperatures. At higher temperatures of around ~900 ^{o}C this trend reverses, and slightly higher CH_4% conversion is observed for increasing amounts of H_2O in the feed.

Figure 21 (b) shows that the CO_2% conversion also decreases with the increasing proportion of steam in the input feed. One might speculate that, as the proportion of steam increases in the feed, the probability that both the SRM and DRM reactions (eqn: 1& 2) increases and eventually lead to increased methane conversion. The contrary is in fact observed. The reason for this non-expectant behavior becomes more obvious when methane conversion is looked at in conjunction with the CO_2% conversion and solid carbon deposition in

Figure 22 (c). At lower temperatures, both CH_4 and CO_2% conversions follow similar decreasing trends with increasing steam. We postulate that this may be due to the competition between DRM and SRM at lower temperatures caused due to the strong endothermicity of both the reactions. Similar analysis of steam addition to DRM reaction had previously been done by Özkara et al.[12], but their analysis presented the equilibrium results without considering solid coke formation. In view of the fact that a considerably higher amount of carbon deposition is observed over the entire temperature range of 200

°C to 1200 °C, even at a low pressure of 1 bar, exclusion of coke deposition from similar analysis leads to considerable inaccuracies in the obtained results.

The fact that both SRM/DRM reactions are endothermic reactions [equation] presents an added challenge of adding more energy to the system to drive the dual reaction system. Production of steam is also a highly energy intensive process. As can be noted from Figure 22 b, the endothermic intensity of the dual reaction increases quite steadily with the increase in temperature. Though, the energy intensity of the process is a small function of pressure (which needs to be accounted separately in terms of compression costs), energy intensity is a good function of the feed mole ratio, which means more the carbon dioxide and steam fed will lead to more energy requirements.

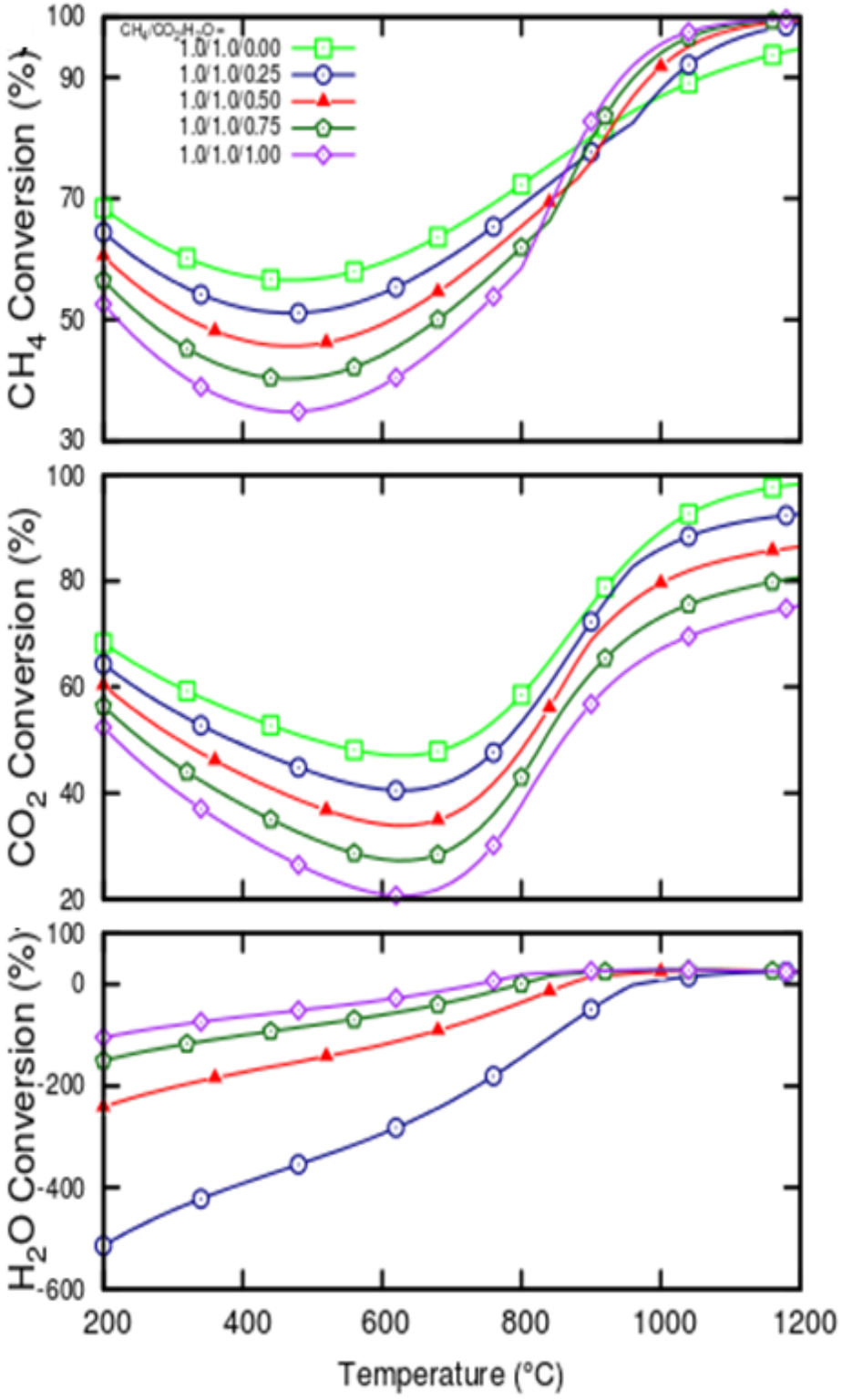

Figure 21 Effect of steam on the % CH_4, CO_2 and H_2O conversion

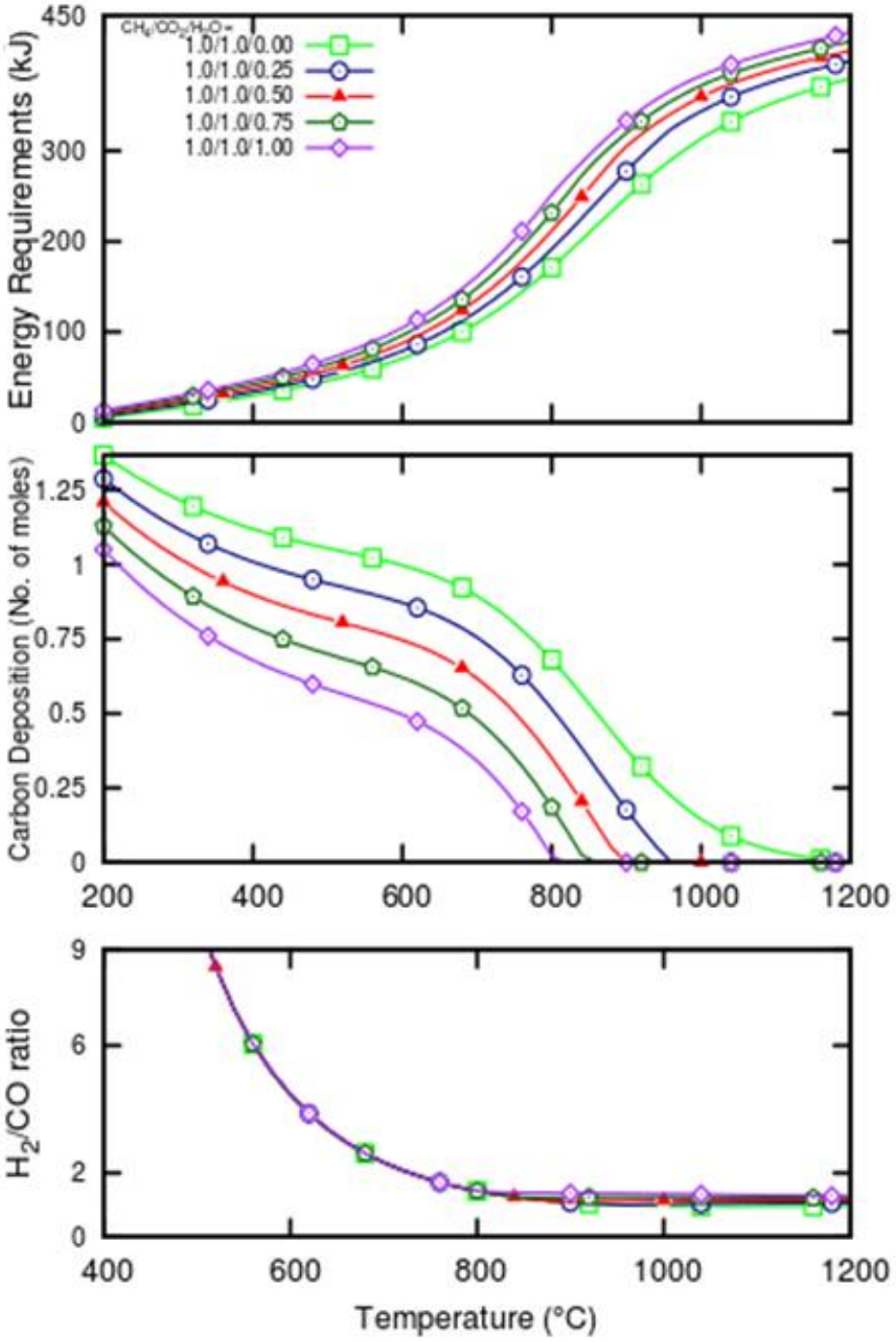

Figure 22 Effect of steam on energy requirements, carbon deposition and syngas ratio

5.1.5 Effect of Oxygen on Dry Reforming Reaction

DRM process is a highly endothermic process in nature. In addition to this, coke deposition during DRM process deactivates the catalyst. To balance these limitations, addition of oxygen to the DRM feed is observed to have notable benefits. Figure 23 illustrates the different performance trends of a typical DRM process when oxygen is added to the process. As can be seen from Figure 23 (a and b), addition of oxygen has a similar effect on both the CH_4 and CO_2 % conversions which are observed to decrease up to 600 °C. This is because WGSR dominates the DRM reaction below 600 °C as shown in Figure 15. With the increase in the oxygen content of the feed, CO_2% and CH_4% conversions are seen to decrease owing to the reason of increased conversion of CH_4 to CO_2 rather than CO. From Figure 24 (a), it can be inferred that the energy requirements decrease continuously with an increase in oxygen content attributing to the presence of POX reaction due to oxygen. A decrease of almost 25 % in carbon formation is observed (Figure 24 (b)) to happen when the oxygen content in the feed is 0.5 mole versus typical DRM condition in absence of oxygen. Similar but less pronounced trend is seen (Figure 24 (c)) in syngas (H_2: CO) yield ratio which eventually damp to almost 1 at all the feed mole ratios.

As a result of this analysis, it can be implied that the presence of oxygen in the feed greatly benefits the energy outlook as well as carbon formation tendency of the DRM process. In particular, an optimized condition at a temperature of 800 °C at 1 bar pressure with oxygen content of 0.5 is expected to operate auto-thermally with almost negligible carbon deposition at a syngas ratio near to 1.5.

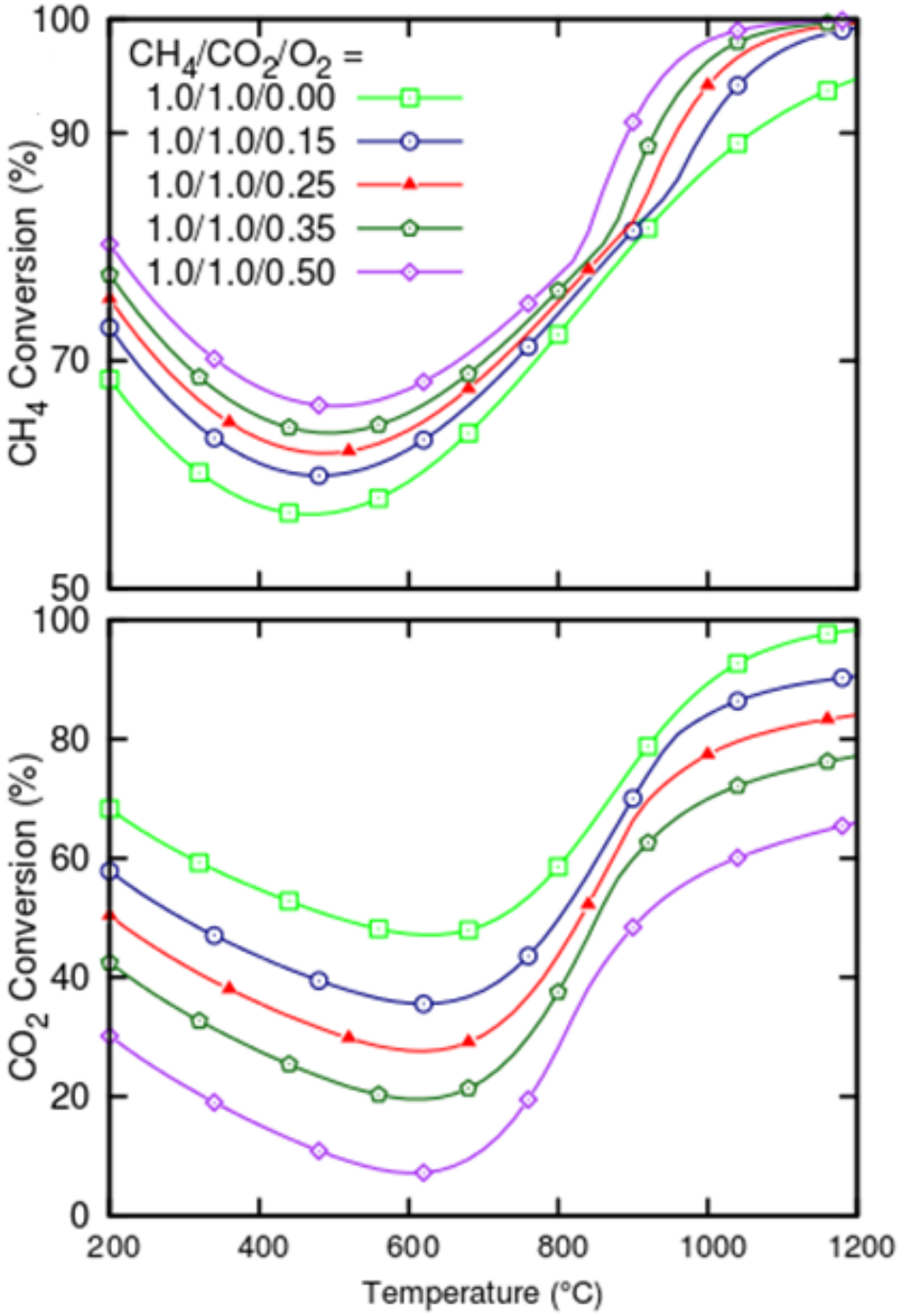

Figure 23 Effect of oxygen on the % CH_4 and % CO_2 conversion

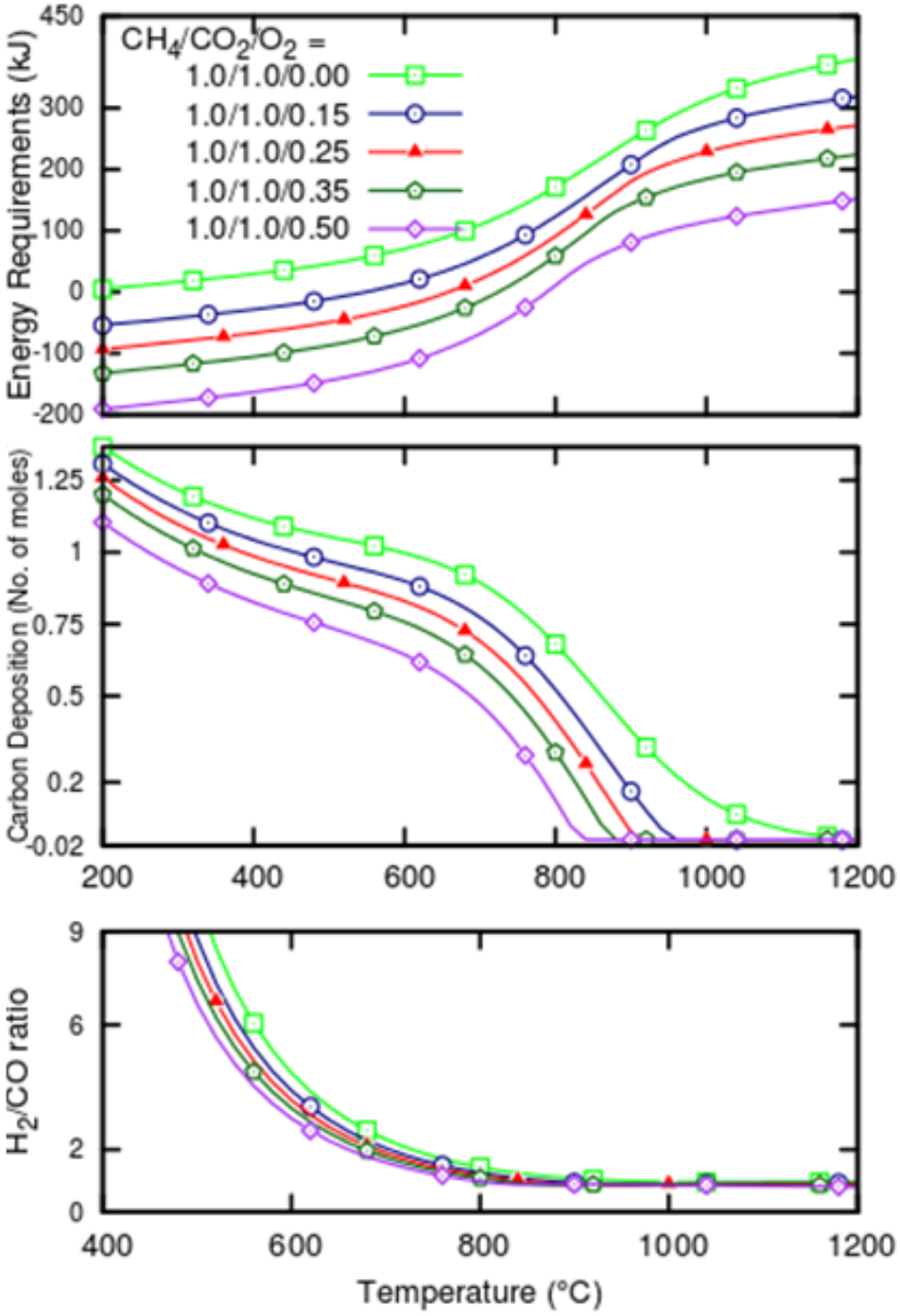

Figure 24 Effect of oxygen on energy requirements, carbon deposition and syngas ratio

5.1.6 Simultaneous Effect of Oxygen & Steam on Dry Reforming Reaction

The addition of steam and oxygen in a CRM process combines all the benefits of the addition of steam and oxygen (as mentioned in section 5.1.4 and section 5.1.5) which, in particular are the increased conversion of methane, reduced carbon deposition and reduced energy requirements on relative basis (to the conventional technologies). Figure 25-28 illustrates the different three-dimensional trends to emphasize on the effect of both the oxidants on the feed conversions. Variation of steam and oxygen simultaneously is helpful in understanding the cumulative effect of both the components and also in finding optimum feed mole ratio. From Figure 27, it can be noticed that the addition of steam and oxygen have an inverse effect on the energy requirement. Low steam and high oxygen content evaluates to the minimum energy requirement of ~82 kJ, on the other hand; it decreases the CO_2 % conversion to a low value of ~48%. Carbon formation is seen (Figure 28) to decrease with increase in both oxygen and steam concentration. This increase offsets the CO_2 % conversion to the lowest value of ~24% and on the other hand, CH_4% conversion increases to the highest value of ~95%. Thus, CO_2 % and CH_4% conversion are seen to have an almost inverse effect by simultaneous increase or decrease of steam and oxygen. From this analysis, an optimum feed mole ratio of CH_4:H_2O:O_2:CO_2 of 1:0.4:0.3:1 is deduced, which gives CO_2% conversion of ~52%, corresponding to energy requirement of 180 kJ with zero carbon deposition.

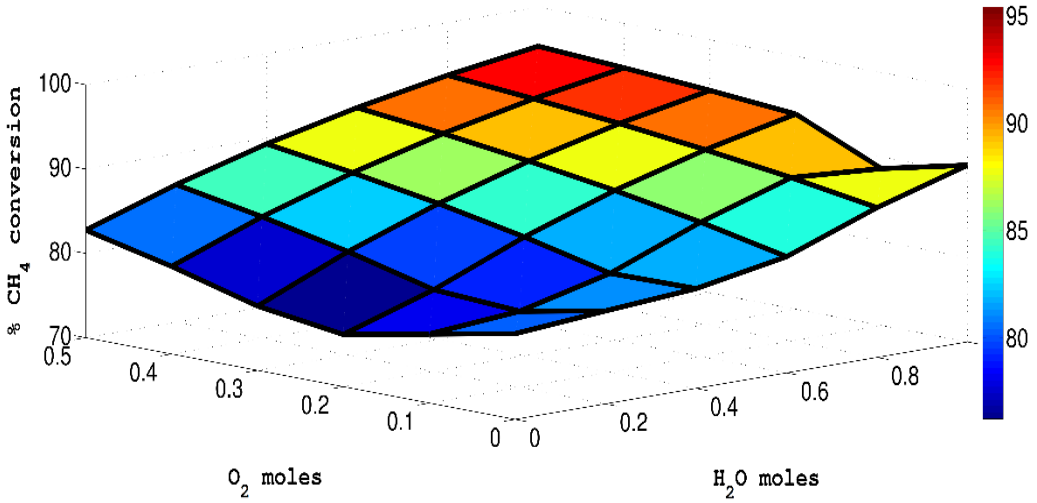

Figure 25 Simultaneous effect of oxygen and steam on % CH_4 conversion

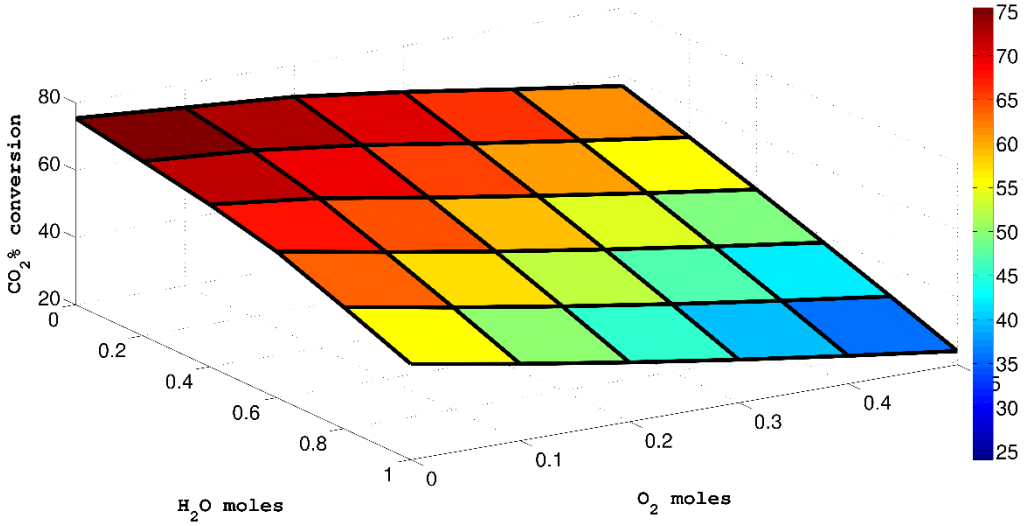

Figure 26 Simultaneous effect of oxygen and steam on % CO_2 conversion

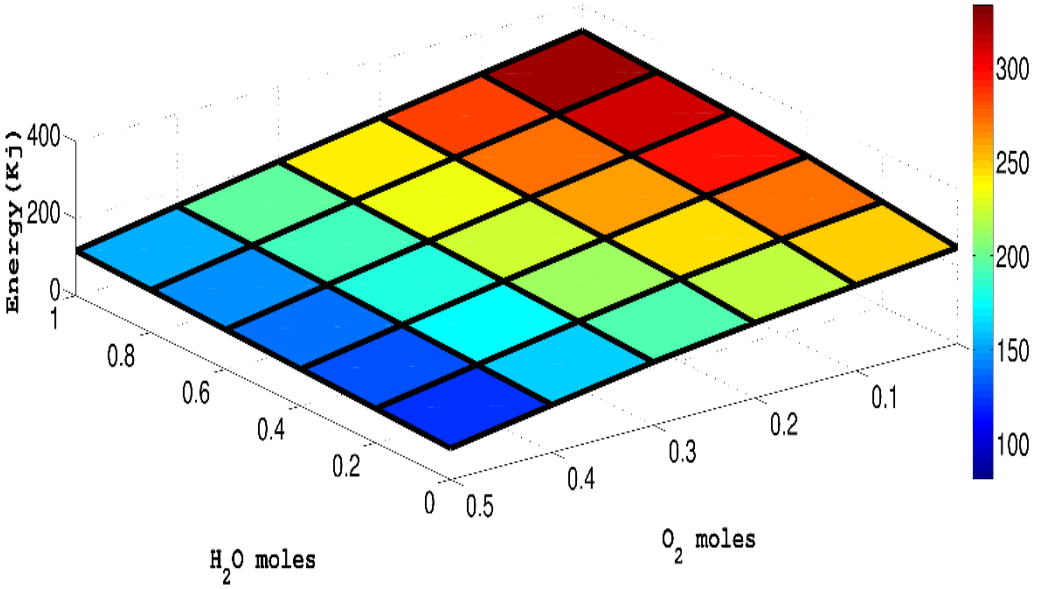

Figure 27 Simultaneous effect of oxygen and steam on energy requirements

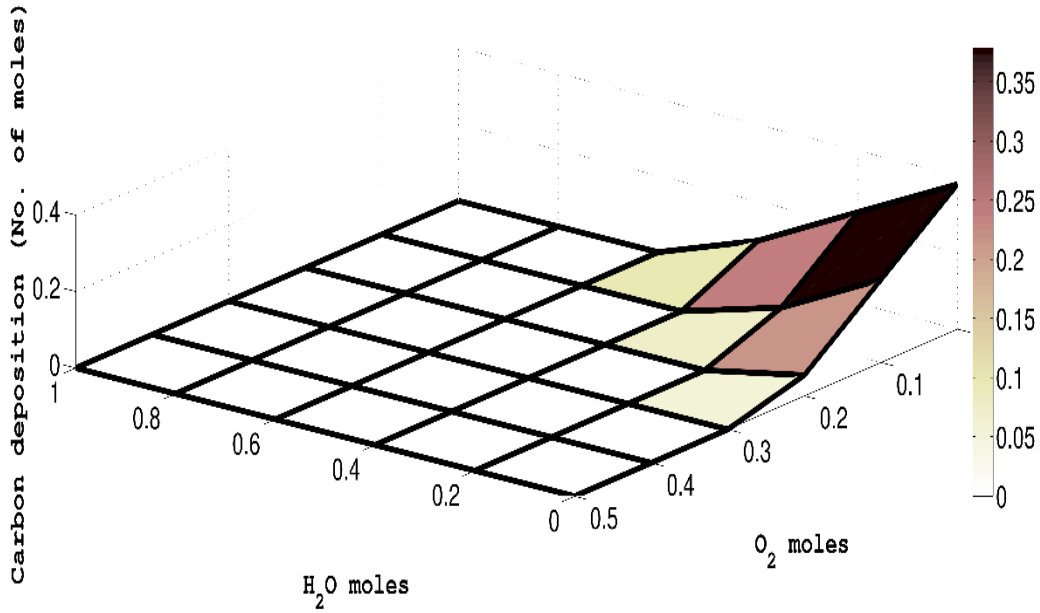

Figure 28 Simultaneous effect of oxygen and steam on carbon deposition

5.2 Fixed Bed Reactor Modeling

Owing to the fact that the reforming reactions are mostly heterogeneous reactions, kinetic limitations are always seen to affect the performance of the system. The condition of the system in bulk phase is always different from the conditions inside the pore of the catalyst due to the presence of transport limitations which in turn effects the product distribution. There have been numerous studies in the literature with an objective to understand such behaviors and to accurately predict the product distribution in the reformer operating conditions. However, these studies have been limited to either kinetics or thermodynamics individually. In the present work, a combined thermodynamic and kinetic study of the various reforming processes and their synergistic blends are studied in the hope to be able to address the shortcomings of any individual reforming technology. This combined thermo-kinetic approach has provided us an oppurtunity to observe the role of the reaction parameters on the reformer behavior meanwhile comparing the thermodynamic analysis and kinetic analysis. Such comparison provides as well an assessment of the validity of the different kinetic models to identify the most appropiate one to be employed in our reformer reactor model.

Xu et al.[30] is a well known study on determing appropiate kinetics model for SRM reaction accompanied by WGSR on Nickel based catalyst ($Ni/MgAl_2O_4$) using intrinsic rate expressions. In their work, they derived three rate equations by using rigorous model discrimination and parameter estimation technique for about two hundred twenty runs of experiment. These rate expression in equation (28) were derived based on the fact

that external diffusion and heat transfer limitations are negligible, which they proved to be the case from their experimental findings.

A similar rate expression (31) for DRM reaction was developed by Verykios et al.[31] for another Nickel based catalyst (Ni/La_2O_3). In their kinetic study, integral and differential reactions were conducted on an experimental setup similar to Xu et al. [30]. Verykios et al.'s model [31] and is based on the assumption that methane activation takes place at catalyst surface and it has also been considered as the rate determining step.

In published literature, there are many studies available on the thermodynamic investigations of a combined DRM/SRM reforming reaction; however, only few studies exist on the kinetic investigations [47] specifically for combined DRM/SRM CRM system. In the present work, we have performed an initial analysis to check the feasibility of a combined DRM/SRM kinetic model based on the existing individual kinetic models presently available in the literature [30] [31]. Though there are many challenges related to such a task, but any success in this presents huge benefits in the overall thermodynamic/kinetic analysis. One of the issues that needs to be considered is the assumptions used in the derivation of each model and their validity in the resulting process. Another concern is the temperature and pressure conditions over which individual models are derived and are expected to be valid. Upon integration of the two models, the calculated product distribution can be used as pre experimental results and also used for a simulation study of combined DRM/SRM reformer in the process simulators. This model will also allow us to accurately understand the regimes of kinetic limitations and its

deviation from thermodynamic predictions for a combined DRM/SRM reaction process following its successful validation as described in section 4.2 (page 31).

In the following section on the simulation of the pseudo-homogeneous fixed bed reactor, details of the product profile of the fixed bed reactor are shown which presents a good basis for initial calculations for the designing of an experimental scale fixed bed reactor for catalyst development.

5.2.1 Pseudo Homogeneous Fixed Bed Reactor

As mentioned previously, the main aim of the simulation of a pseudo homogeneous fixed bed reactor is to use its results as a preliminary data for the designing of the experimental reactor setup. The advantage of this study is that it gives information on the product distribution of the reacting compounds as a function of reactor length. This also gives inferences on the pressure drop and the temperature profile across the reactor which is necessary for sizing of the experimental reactor. In the following section on the modeling of an industrial reactor, a case example of the industrial reformer specification is simulated to illustrate the product distribution and the corresponding temperature and pressure profiles. In the final section 5.2.1.2 (page 65), a similar example for a lab scale reactor is shown, results of which will be used for future experimental work.

5.2.1.1 Illustrative example of Industrial reactor simulation

In this study, a fixed bed reactor with pseudo homogeneous reactor dynamics is simulated in which the radial gradients are neglected. As a case example of the industrial reformer, temperature and feed pressure data are adopted from the literature [30, 48]. Figure 29-31 shows the product distribution, temperature profile and the pressure drop

profile of the combined DRM/SRM reaction mixture using the combined DRM/SRM reaction model as described in section 3.2.2 (page 23) for the following feed conditions:

Table 5 Industrial reactor specifications

Reactor operating conditions	
Feed temperature	800 K
Reactor wall temperature	1123 K
Reactor tube diameter	0.0795 m
Feed gas pressure	28.37 bar
$CH_4/H_2O/CO_2$ feed ratio	1.5:1:1
Feed flow	3500 mol/hr
Catalyst specifications	
Bulk density	946.8 kg/m^3
Porosity	0.5319
Particle diameter	0.01741 m

Figure 29 shows the product distribution of the reformer reaction mixture. It can be observed from this that the molar flow rate of hydrogen and carbon monoxide increases while that of methane, steam and carbon dioxide decreases along the bed length. A steady composition is observed to be reached after a bed length of 0.1 m, this however depends upon the initial feed composition. Due to the effective equilibrium limitation at a temperature of 1173 K, a maximum conversion of about ~70% is seen for carbon dioxide and methane conversions, this however can be improved by increasing the reactor wall temperature which drives the reaction in a more thermodynamically favorable conversion level. Steam conversion is however seen to be less (~40%) compared to methane and carbon dioxide conversions, which could be attributed again to the thermodynamic

limitations which are discussed in section 5.1 on thermodynamic analysis (page 33). As the feed temperature (800 K) is less than the reactor wall temperature (1173 K), the temperature profile (Figure 30) increases through the length of the bed and reaches a steady value of the wall temperature. A steady change is also noted for the pressure drop (Figure 31) across the bed length.

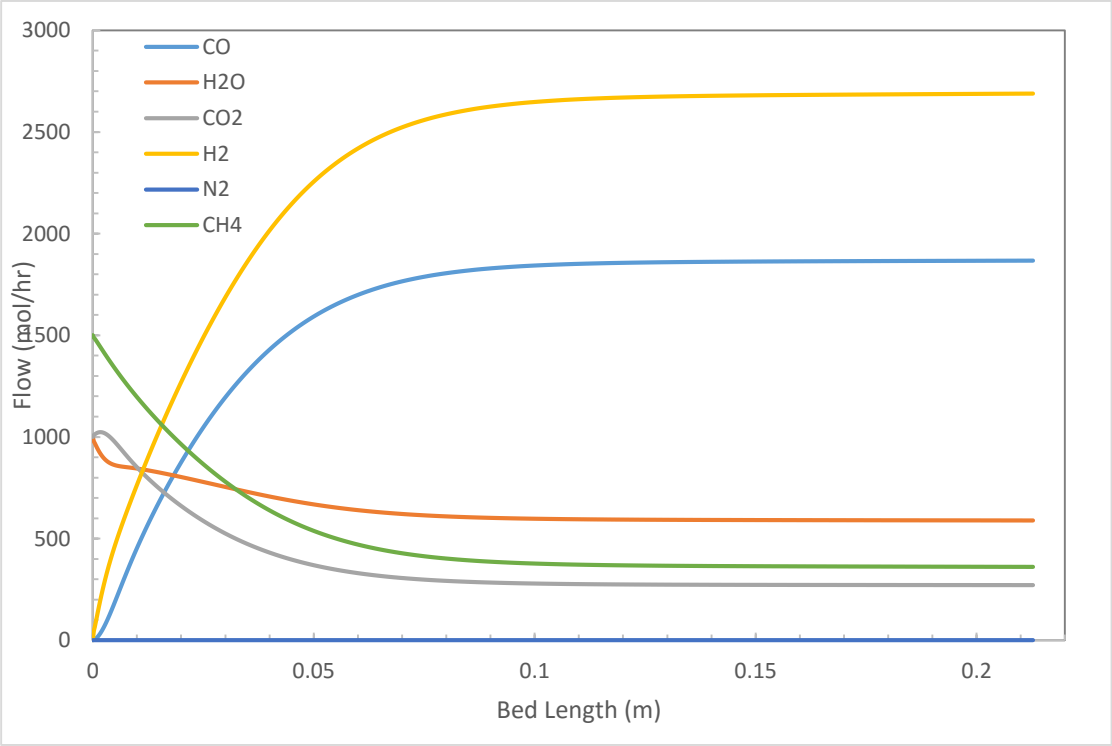

Figure 29 Product distribution along the bed of fixed bed reactor

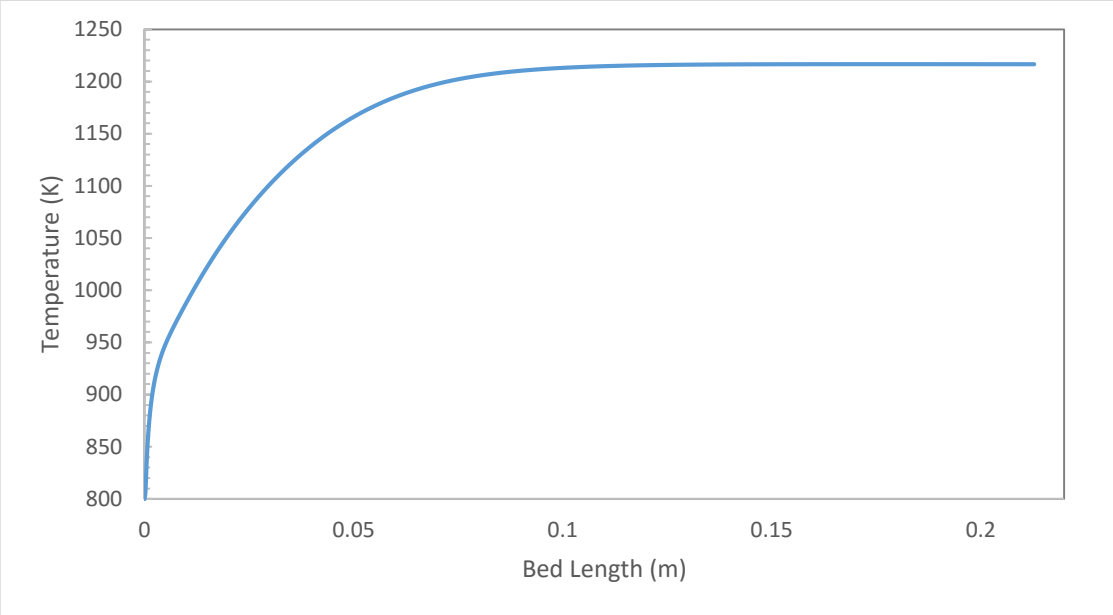

Figure 30 Temperature profile across the length of the reactor

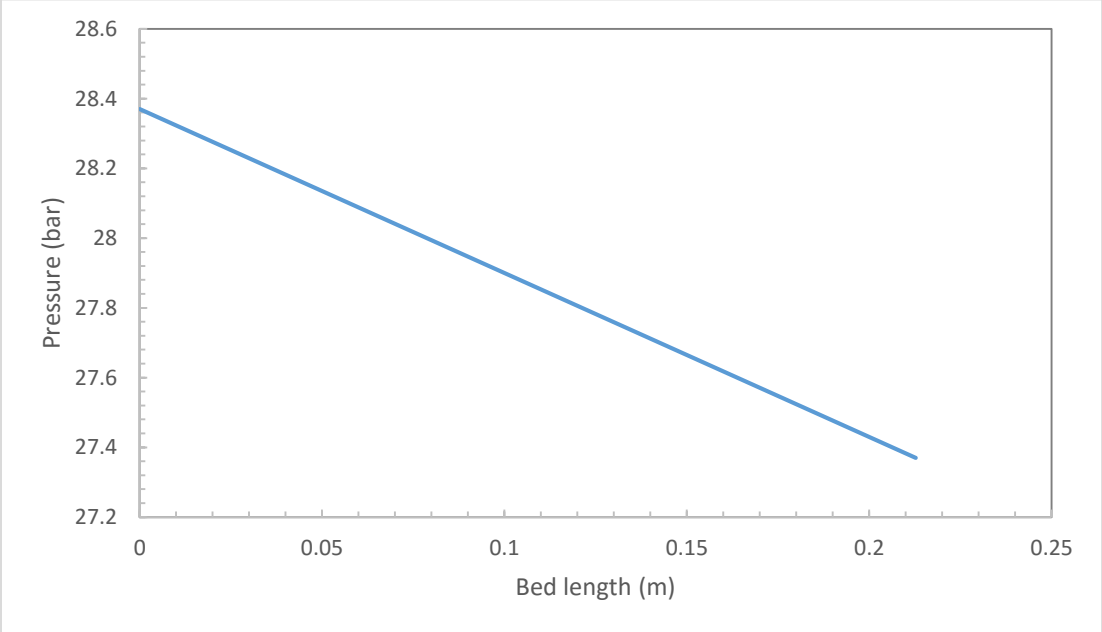

Figure 31 Pressure drop across the length of the reactor

The above mentioned analysis is an example to show the effect of the feed condition and the reactor temperatures. There are however many other parameters like the specification of the catalyst and the reactor dimensions that effect the product distribution, temperature and the pressure profile of the reactor as described above.

5.2.1.2 Illustrative example of Lab scale reactor simulation

Similar to the results shown in the previous section, in this section the results related to the simulation of the lab scale reactor will be shown. Typically the dimension of the lab scale reactor is many times smaller than the dimension of the industrial reactor including the flow of the reactants that are handled. The advantage of a lab scale reactor is to provide a platform for development of new catalyst, or for other process modification purposes. All the industrial scale reactors are developed only after preliminary experimental work carried out in a lab scale or bench scale plant. In this study, the proposed fixed bed reactor script was developed to aid in the designing of the fixed bed reactor which will be used in further experimental work on the scale up studies for a new class of catalyst which are highly resistant to coke deposition.

Following are the proposed specification of the lab scale reactor by the experimental team of our research group which are involved in the designing of the bench scale reactor for the catalytic study as a part of future experimental campaign:

Table 6 Lab scale reactor specification

Reactor operating conditions	
Feed temperature	800 K
Reactor wall temperature	1123 K
Reactor tube diameter	0.02 m
Feed gas pressure	4 bar
$N_2/CH_4/H_2O/CO_2$ feed ratio	0.05:0.25:0.1:0.175
Feed flow	0.575 mol/hr
Catalyst specifications	
Bulk density	946.8 kg/m^3
Porosity	0.5319

Figure 32-34 shows the product distribution, temperature profile and the pressure profile of the fixed bed reactor based on the above mentioned reactor specifications. These profiles can be generated for any specified reactor, catalyst and feed specification and thus would serve to aid further experimental studies. Figure 35 shows a proposed lab scale reactor set up that would be used in the above mentioned experimental study.

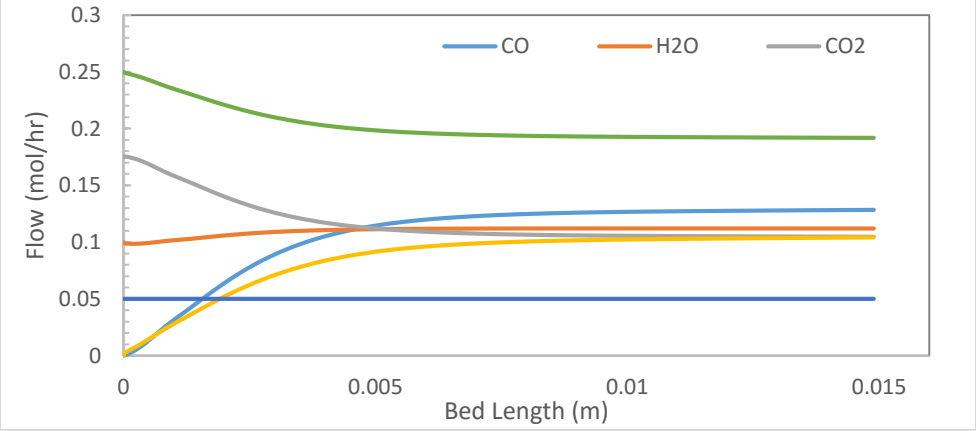

Figure 32 Product distribution of a Lab scale reactor

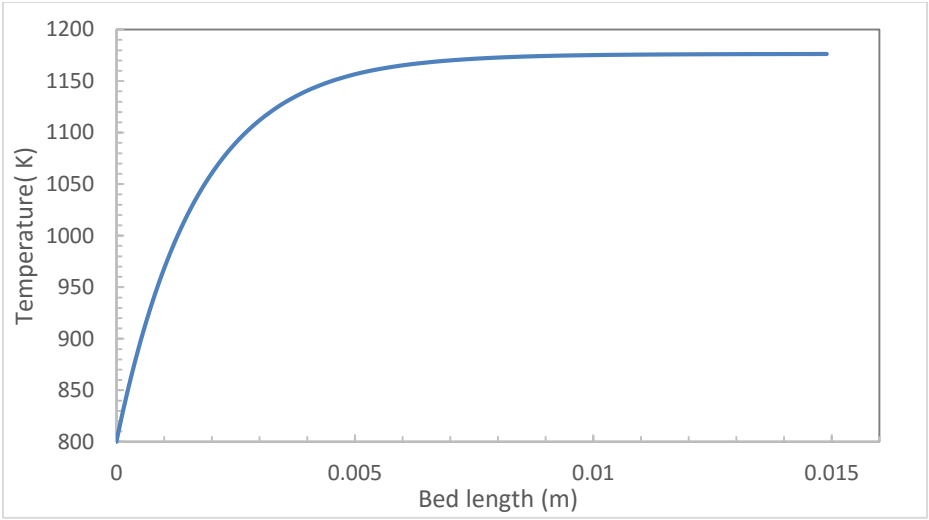

Figure 33 Temperature profile of a lab scale reactor

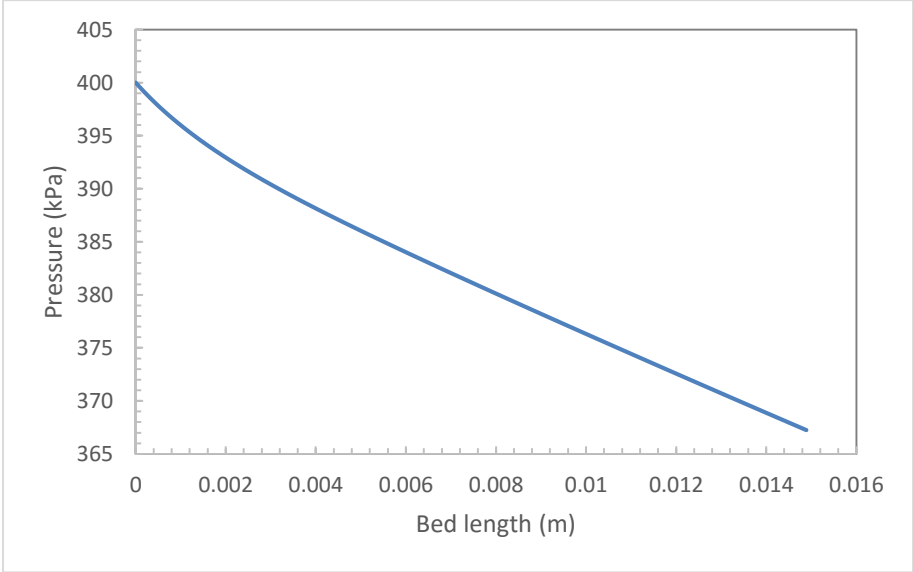

Figure 34 Pressure drop across a lab scale fixed bed reactor

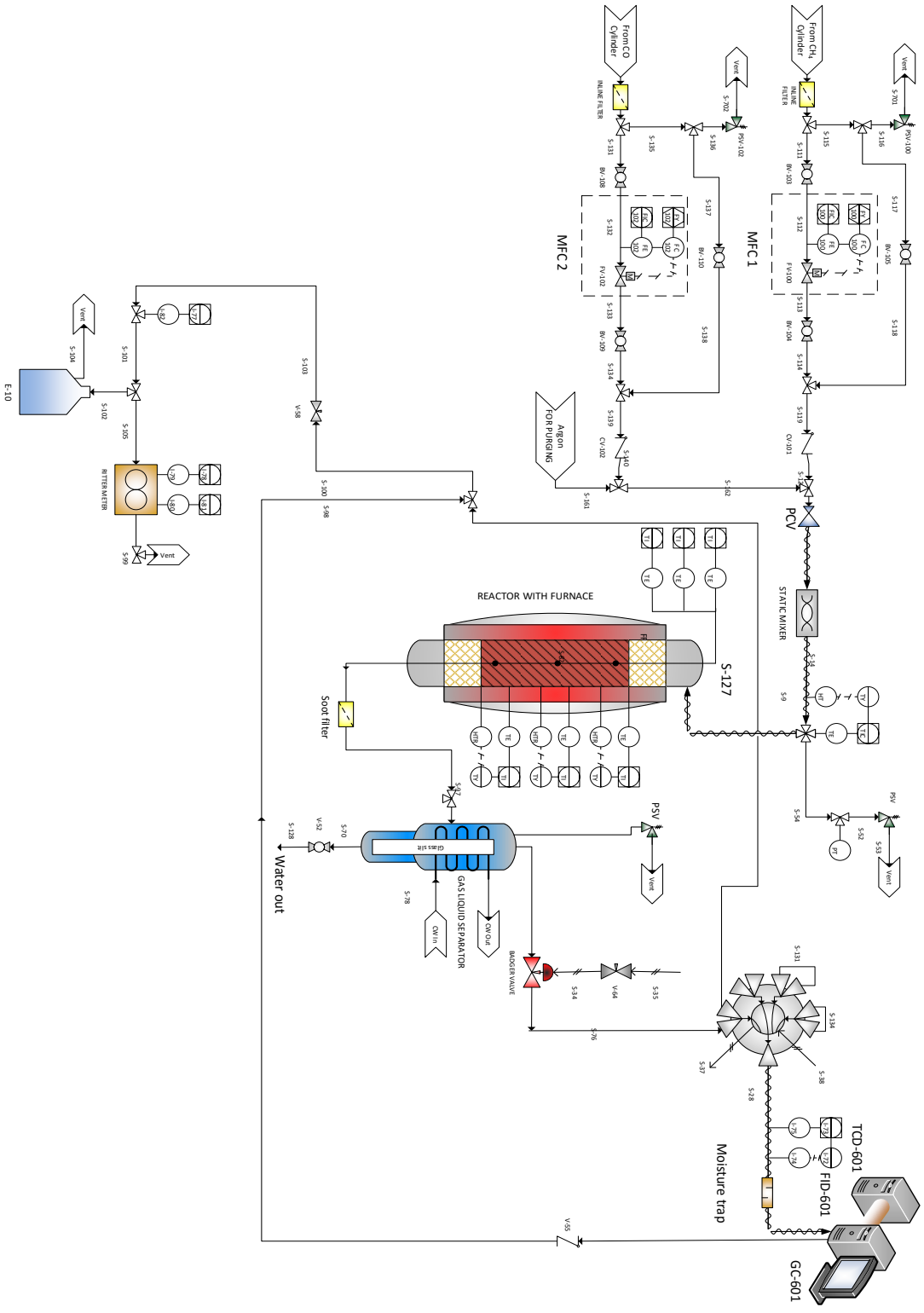

Figure 35 Experimental set up for catalyst development studies

CHAPTER VI

CONCLUSION AND FUTURE WORK

This study by far covers various aspects of the designing and simulation of a combined reforming of methane reactor. To address the problem of CO_2 emissions, dry reforming of methane is given increased attention in many of the recent studies; however the challenges related to dry reforming like the coke deposition and high energy requirements are crucial concerns that need to be addressed. The two most important ways to tackle the challenges related to dry reforming of methane include combined reforming and development of better catalyst for improved activity. In this work a comprehensive study of the effect of different process conditions that aid in controlling the inherent process limitations of dry reforming was successfully conducted using thermodynamic analysis. It was observed that high temperature and low pressure reaction are favorable for higher conversions of carbon dioxide. The effect of addition of oxygen and steam have also been investigated along with accountability of energy requirements in the entire process. An optimized feed condition was successfully derived by careful observation of the different tradeoffs that effect the system. High pressure operation of the industrial reformer was very often considered as ideal gas condition, however in this study a detailed analysis of the non-ideality associated at high pressure operation has been accounted using various equations of state (Peng Robinson, Soave Redlich Kwong and Redlich Kwong). Further to thermodynamic studies, kinetic modeling was also carried out for a combined dry and steam reforming reaction. Existing steam reforming and dry reforming reactions were also successfully combined and validated against the equilibrium results with high

level of accuracy. The developed combined model was then successful incorporated in simulation of a pseudo homogeneous fixed bed reactor, results of which are being used for the development and designing of an experimental lab scale reforming reactor set up which will be used for future catalyst scale up studies.

As an immediate future extension to this study, there is a need to improve the 1-dimensional pseudo-homogeneous fixed bed reactor model to a 2-dimensional model which will incorporate the radial profiles along the bed. Any improvement in this model would serve to improve the accuracy of the obtained results. There is also a need to further test the proposed dry/steam reforming coupled model along with partial oxidation and carbon deposition models available in published literature. This would be helpful in extending the work from a bi-reforming scale to a tri-reforming scale and thus cover the complete range of simulation analysis. In addition to the aforesaid studies, improvements in the kinetic parameters can be made by regression analysis to test if the proposed combination could provide satisfactory results for different variety of catalysts. Thus this study opens a plethora of possibilities which upon exploration could provide much better clarity in understanding and tackling the limitations of a combined reforming reaction.

REFERENCES

[1] Ross, J.R.H., et al., *The catalytic conversion of natural gas to useful products.* Catalysis Today, 1996. **30**: p. 193–199.

[2] Pakhare, D. and J. Spivey, *A review of dry (CO2) reforming of methane over noble metal catalysts.* Chemical Society Reviews, 2014. **43**(22): p. 7813-7837.

[3] Ehlinger, V.M., et al., *Process design and integration of shale gas to methanol.* ACS Sustainable Chemistry & Engineering, 2013. **2**(1): p. 30-37.

[4] Bao, B., M.M. El-Halwagi, and N.O. Elbashir, *Simulation, integration, and economic analysis of gas-to-liquid processes.* Fuel Processing Technology, 2010. **91**(7): p. 703-713.

[5] Gadalla, A.M. and B. Bower, *The Role of Catalyst Support on the Activity of Nickel for Reforming Methane with Co2.* Chemical Engineering Science, 1988. **43**(11): p. 3049-3062.

[6] Wilhelm, D., et al., *Syngas production for gas-to-liquids applications: technologies, issues and outlook.* Fuel Processing Technology, 2001. **71**(1): p. 139-148.

[7] Arouri, M.E.H., et al., *Energy consumption, economic growth and CO2 emissions in Middle East and North African countries.* Energy Policy, 2012. **45**: p. 342-349.

[8] Djaidja, A., et al., *Characterization and activity in dry reforming of methane on NiMg/Al and Ni/MgO catalysts.* Catalysis Today, 2006. **113**: p. 194–200.

[9] Nagaoka, K., et al., *Carbon Deposition during Carbon Dioxide Reforming of Methane—Comparison between Pt/Al_2O_3 and Pt/ZrO_2.* Journal of Catalysis, 2001. **197**: p. 34-42.

[10] Ross, J.R.H., *Natural gas reforming and CO_2 mitigation.* Catalysis Today, 2005. **100**: p. 151–158.

[11] Noureldin, M.M.B., N.O. Elbashir, and M.M. El-Halwagi, *Optimization and Selection of Reforming Approaches for Syngas Generation from Natural/Shale Gas.* Industrial & Engineering Chemistry Research, 2014. **53**(5): p. 1841-1855.

[12] Özkara-Aydınoğlu, Ş., *Thermodynamic equilibrium analysis of combined carbon dioxide reforming with steam reforming of methane to synthesis gas.* International Journal of Hydrogen Energy, 2010. **35**(23): p. 12821-12828.

[13] Nematollahi, B., et al., *Thermodynamic analysis of combined reforming process using Gibbs energy minimization method: In view of solid carbon formation.* Journal of Natural Gas Chemistry, 2012. **21**(6): p. 694-702.

[14] Noureldin, M.M., et al., *A Process Integration Approach to the Assessment of CO2 Fixation through Dry Reforming.* ACS Sustainable Chemistry & Engineering, 2015. **3**(4): p. 625-636.

[15] Baltrusaitis, J. and W.L. Luyben, *Methane Conversion to Syngas for Gas-to-Liquids (GTL): Is Sustainable CO2 Reuse via Dry Methane Reforming (DMR) Cost Competitive with SMR and ATR Processes?* ACS Sustainable Chemistry & Engineering, 2015. **3**(9): p. 2100-2111.

[16] Luyben, W.L., *Design and Control of the Dry Methane Reforming Process.* Industrial & Engineering Chemistry Research, 2014. **53**(37): p. 14423-14439.

[17] Zhang, Y., et al., *Thermodynamic analyses of tri-reforming reactions to produce syngas.* Energy & Fuels, 2014. **28**(4): p. 2717-2726.

[18] Chein, R., et al., *Thermodynamic analysis of dry reforming of CH 4 with CO 2 at high pressures.* Journal of Natural Gas Science and Engineering, 2015. **26**: p. 617-629.

[19] Amin, N.A.S. and T.C. Yaw, *Thermodynamic equilibrium analysis of combined carbon dioxide reforming with partial oxidation of methane to syngas.* International Journal of Hydrogen Energy, 2007. **32**(12): p. 1789-1798.

[20] Nikoo, M.K. and N. Amin, *Thermodynamic analysis of carbon dioxide reforming of methane in view of solid carbon formation.* Fuel Processing Technology, 2011. **92**(3): p. 678-691.

[21] Liu, S., et al., *Thermodynamic analysis of hydrogen production from oxidative steam reforming of ethanol.* Energy & Fuels, 2008. **22**(2): p. 1365-1370.

[22] Wang, X., et al., *Thermodynamic analysis of glycerin steam reforming.* Energy & Fuels, 2008. **22**(6): p. 4285-4291.

[23] Faungnawakij, K., R. Kikuchi, and K. Eguchi, *Thermodynamic analysis of carbon formation boundary and reforming performance for steam reforming of dimethyl ether*. Journal of Power Sources, 2007. **164**(1): p. 73-79.

[24] Semelsberger, T.A. and R.L. Borup, *Thermodynamic equilibrium calculations of dimethyl ether steam reforming and dimethyl ether hydrolysis.* Journal of Power Sources, 2005. **152**: p. 87-96.

[25] Song, C., et al., *Tri-reforming of methane over Ni catalysts for CO 2 conversion to syngas with desired H 2/CO ratios using flue gas of power plants without CO 2 separation.* Studies in Surface Science and Catalysis, 2004. **153**: p. 315-322.

[26] Choudhary, V.R., et al., *Carbon-free dry reforming of methane to syngas over NdCoO 3 perovskite-type mixed metal oxide catalyst.* Catalysis Letters, 2005. **100**: p. 271-276.

[27] Choudhury, V.R. and K.C. Mondal, *CO2 reforming of methane combined with steam reforming or partial oxidation of methane to syngas over NdCoO3 perovskite-type mixed metal-oxide catalyst.* Applied Energy, 2006. **83**: p. 1024-1032.

[28] Lee, S.-H., et al., *Tri-reforming of CH4 using CO2 for production of synthesis gas to dimethyl ether.* Catalysis Today, 2003. **87**(1): p. 133-137.

[29] Freitas, A.C. and R. Guirardello, *Thermodynamic analysis of methane reforming with CO2, CO2+ H2O, CO2+ O2 and CO2+ air for hydrogen and synthesis gas production.* Journal of CO2 Utilization, 2014. **7**: p. 30-38.

[30] Xu, J. and G.F. Froment, *Methane steam reforming, methanation and water-gas shift: I. Intrinsic kinetics.* AIChE Journal, 1989. **35**(1): p. 88-96.

[31] Verykios, X.E., *Catalytic dry reforming of natural gas for the production of chemicals and hydrogen.* International Journal of Hydrogen Energy, 2003. **28**(10): p. 1045-1063.

[32] Hou, K. and R. Hughes, *The kinetics of methane steam reforming over a Ni/α-Al 2 O catalyst.* Chemical Engineering Journal, 2001. **82**(1): p. 311-328.

[33] Olsbye, U., T. Wurzel, and L. Mleczko, *Kinetic and reaction engineering studies of dry reforming of methane over a Ni/La/Al2O3 catalyst.* Industrial & Engineering Chemistry Research, 1997. **36**(12): p. 5180-5188.

[34] Ahmed, K. and K. Foger, *Kinetics of internal steam reforming of methane on Ni/YSZ-based anodes for solid oxide fuel cells.* Catalysis Today, 2000. **63**(2): p. 479-487.

[35] Iyer, M.V., et al., *Kinetic modeling for methane reforming with carbon dioxide over a mixed-metal carbide catalyst.* Industrial & Engineering Chemistry Research, 2003. **42**(12): p. 2712-2721.

[36] Abbott, M., J. Smith, and H. Van Ness, *Introduction to chemical engineering thermodynamics* 2001: McGraw-Hill.

[37] Froment, G.F., K.B. Bischoff, and J. De Wilde, *Chemical reactor analysis and design*. Vol. 2. 1990: Wiley New York.

[38] Fogler, H.S., *Elements of chemical reaction engineering.* 1999.

[39] Ergun, S. and A.A. Orning, *Fluid flow through randomly packed columns and fluidized beds.* Industrial & Engineering Chemistry, 1949. **41**(6): p. 1179-1184.

[40] Khalesi, A., H.R. Arandiyan, and M. Parvari, *Effects of Lanthanum Substitution by Strontium and Calcium in La-Ni-Al Perovskite Oxides in Dry Reforming of Methane.* Chinese Journal of Catalysis, 2008. **29**(10): p. 960-968.

[41] Liu, D., et al., *Carbon dioxide reforming of methane to synthesis gas over Ni-MCM-41 catalysts.* Applied Catalysis A: General, 2009. **358**(2): p. 110-118.

[42] Cui, Y., et al., *Kinetic study of the catalytic reforming of CH4 with CO2 to syngas over Ni/α-Al2O3 catalyst: The effect of temperature on the reforming mechanism.* Applied Catalysis A: General, 2007. **318**: p. 79-88.

[43] Rao, Y. and K. Narayanan, *Introduction to chemical engineering thermodynamics*, 2001, Universities Press: Hyderabad, India.

[44] Soave, G., *Equilibrium constants from a modified Redlich-Kwong equation of state.* Chemical Engineering Science, 1972. **27**(6): p. 1197-1203.

[45] Peng, D.-Y. and D.B. Robinson, *A new two-constant equation of state.* Industrial & Engineering Chemistry Fundamentals, 1976. **15**(1): p. 59-64.

[46] Bartholomew, C.H. and R.J. Farrauto, *Fundamentals of Industrial Catalytic Processes* 2006: Wiley.

[47] Shahkarami, P. and S. Fatemi, *Mathematical Modeling and Optimization of Combined Steam and Dry Reforming of Methane Process in Catalytic Fluidized Bed Membrane Reactor.* Chemical Engineering Communications, 2015. **202**(6): p. 774-786.

[48] Elnashaie, S.S. and F. Uhlig, *Numerical Techniques for Chemical and Biological Engineers Using MATLAB®: A Simple Bifurcation Approach* 2007: Springer Science & Business Media.

APPENDIX A

MATLAB CODE

In order to calculate all the results discussed in this thesis, the following codes were developed in MATLAB®.

FOR THERMODYNAMIC STUDY:

```
clc;
clear;
warning('off','all');
imole=0;
Systemcomp=[1,27,28,29,30,32,47];
ch1=Systemcomp;
dummy=size(ch1);
n=dummy(2);
imole=[3561,14076,0,0,18768,0,0];
R=8.314;
T=298.15;
t11=[1173,50,1173];
p0=1;
P=28.43;
compoundnames={'Methane';'Ethane';'propane';'n-Butane';'n-pentane';'n-hexane';'n-heptane';'n-
octane';'ethylene';'propylene';'1-Butene';'1-Pentene';'1-Hexene';'1-Heptene';'Acetaldehyde
';'Acetylene';'Benzene(g)';'3-
Butadiene';'Cyclohexane(g)';'Ethanol';'Ethylbenzene';'EthyleneOxide';'Formaldehyde';'Methanol(g)';'Styre
ne';'Toluene(g)';'water';'oxygen';'carbon
monoxide';'carbondioxide';'carbondisulphide';'hydrogen';'nitrogen';'chlorine';'hydrogen sulphide';'sulphur
```

```
di oxide';'sulphur tri oxide';'nitric oxide';'hydrogen chloride';'hydrogen
cyanide';'ammonia';'Glycerol';'Crude Glycerol';'Acetol';'Acetaldehyde';'Formaldehyde';'Carbon'};
eos=3;              %   This to set PR EOS
ch=eos;
[ta,atoms,X,data,G,x1]=options11(ch1,n,imole);
totatoms=imole*atoms';          % This is to set the no. of atoms of each element in the feed
[ta,atoms,X,data,G,x1]=options11(ch1,n,imole);
for i=1:n
   data(1,i)=ch1(i);
end
for i=(n+1):(n+4)
   data(1,i)=0;
end
l=1;
for loop=t11(1):t11(2):t11(3)
   T1=loop;
   moles=0;
   for i=1:n
      for j=1:9
         x2(j)=x1(i,j);
      end
      [G(i),phi(i)]=specie(n,T,T1,P,p0,x2,ch);

   end
```

```
    for i=1:n
        for j=1:n
            if i==j
                moles(i,j)=1;
            end
        end

    end
atom1=atoms';
        [z,v]=newsolvingnew(n,X,ta,moles,R,T1,phi,G,atom1,atoms,totatoms,P,p0,ch1);
    X=z;
    SUM=sum(z);
    for i=1:n
        z(i)=z(i)/SUM;
    end
    for j=1:n
        data(l,j)=z(j);
    end
    temperatureforplot(l)=loop;
    l=l+1;
end
newdata=0;
for m=1:n
    for o=1:(l-1)
        newdata(o,m)=data(o,m);
    end
```

```
end
[m5]=molematrix(atom1,newdata,totatoms);
[energypertemp1]=energycalculator(x1,t11,n,m5,T,imole,ch1);
   for i=1:n
      legendedcompounds(i)=compoundnames(ch1(i));
   end
%    t=temperatureforplot';
%    en=energypertemp1;
%    write_gnuplot_file(t11,P,imole,m5,t,en);
A=[temperatureforplot',m5,energypertemp1'];


 function [ta,atoms,X,data,G,x1]=options11(ch1,n,imole)


   %dummy=size(totatoms);


   %ta=dummy(2);
ta=3;                % I am fixing the total types of ataoms to Carbon, Oxygen and Hydrogen
   atoms=0;
   M=0;
   for i=1:n
      [M,atomdummy]=compound(ch1(i));
      for j=1:9
         x1(i,j)=M(j);
      end
      for j=1:ta
         atoms(i,j)=atomdummy(j);
```

```
    end
  end

  atoms=atoms';

  X=0;

  for i=1:n
    X(i)=0.5;
  end

%   for i=(n+1):(n+ta+1)
%     X(i)=1;
%   end

  data=0;
  l=1;
  G=0;
end

function [M,atoms]=compound(e1)
  cpm=[-6.567,7.466,-2.164,0.701,190.6,45.99,-74520,-50460,0.012;-12.158,16.417,-
5.561,1.455,305.3,48.72,-83820,-31855,0.1;-17.096,24.784,-8.824,2.229,369.8,42.48,-104680,-
```

24290,0.152;-21.394,31.721,-11.402,3.003,425.1,37.96,-125790,-16570,0.2;-25.885,38.964,-14.111,3.777,469.7,33.7,-146760,-8650,0.252;-30.344,46.142,-16.791,4.551,507.6,30.25,-166920,150,0.301;-34.819,53.354,-19.486,5.3250,540.2,27.4,-187780,8260,0.25;-39.301,60.601,-22.208,6.099,568.7,24.9,-208750,16260,0.4;-8.616,12.008,-4.392,1.548,282.3,50.4,52510,68460,0.087;-13.423,19.127,-6.915,2.322,268.6,46.65,19710,62205,0.14;-18.113,26.858,-9.873,3.096,420,40.43,-540,70340,0.191;-22.429,33.788,-12.447,3.87,0,0,-21280,78410,0;-26.9,41.031,-15.157,4.644,0,0,-41950,86830,0;-31.372,48.237,-17.847,5.418,0,0,-62760,0,0;-15.1865,14.146,-6.158,2.4355,466,55.5,-166190,-128860,0.291;-0.659,-0.012,0,0.342,0,0,227480,209970,0;-20.579,33.172,-13.301,4.923,0,0,82930,129665,0;-14.095,22.436,-8.882,3.189,425.2,42.77,109250,149795,0.19;-33.996,56.091,-20.928,4.644,560.4,43.5,-123140,31920,0.212;-11.5905,16.94,-6.002,1.5685,513.9,61.48,-235100,-168490,0.645;-24.269,48.295,-18.476,5.697,617.2,36.06,29920,130890,0.303;-13.869,20.613,-9.296,1.615,0,0,-52630,-13010,0;-4.5755,5.576,-1.877,0.8875,408,65.9,-108570,-102530,0.282;-7.8775,10.348,-3.45,0.7945,512.6,80.97,-200660,-161960,0.564;2.05,50.192,-16.662,0,636,38.4,147360,213900,0.297;0.29,47.052,-15.716,0,591.8,41.06,50170,122050,0.262;-1.5985,0.775,0,0.1415,647.1,220.55,-241818,-228572,0.345;0,0,0,0,154.6,50.43,0,0,0.022;-0.2145,-0.467,0,0.9495,132.9,34.99,-110525,-137169,0.048;0.047,-0.232,0,-0.063,304.2,73.83,-393509,-394359,0.224;-3.688,3.49,0,1.527,552,79,0,0,0.111;0,0,0,0,33.19,13.13,0,0,-0.216;0,0,0,0,126.2,34,0,0,0.038;0,0,0,0,417.2,77.1,0,0,0.069;-3.432,2.796,0,0.458,373.5,89.63,-20630,-33560,0.094;-2.054,2.203,0,-0.005,430.8,78.84,-296830,-300194,0.245;-1.5125,2.025,0,-0.9045,490.9,82.1,-441040,0,0.424;-5.3515,-0.723,0,0.3145,180.2,64.8,90250,86550,0.583;-2.9105,0.223,0,0.4485,324.7,83.1,-92307,-95299,0.132;4.736,1.359,0,-0.725,456.7,53.9,135100,1247100,0.41;-4.5755,1.794,0,-0.3655,405.7,112.8,-46110,-16450,0.253;-24.8195,-4.701973,-0.038973,2.5695,723,40,-528.8,-448.49,1.32;-22.21541,-2.54020705,-0.51612705,2.29672,692.785,47.5413,-30960.06,25341.3365,1.20441;-30.23849296,-8.06724E-05,-0.000121009,0,595.15,57.4,0,0,0.77358;7.71971845,-6.71685E-05,-0.000100753,0,461,55.7,0,0,0.303;23.4987753,1.99156E-05,2.98734E-05,0,407,65.9,0,0,0.25299;0,0,0,0,6810,2230,0,0,0.326841];

```
    %delta values


atomdatabase=[1,0,4,0,0,0;2,0,6,0,0,0;3,0,8,0,0,0;4,0,10,0,0,0;5,0,12,0,0,0;6,0,14,0,0,0;7,0,16,0,0,0;8,0,18,
0,0,0;2,0,4,0,0,0;3,0,6,0,0,0;4,0,8,0,0,0;5,0,10,0,0,0;6,0,12,0,0,0;7,0,14,0,0,0;3,1,6,0,0,0;2,0,2,0,0,0;6,0,6,0
,0,0;4,0,6,0,0,0;6,0,12,0,0,0;2,1,6,0,0,0;7,0,8,0,0,0;2,1,4,0,0,0;1,1,2,0,0,0;1,1,4,0,0,0;0,0,0,0,0,0;6,0,7,1,0,0
;0,1,2,0,0,0;0,2,0,0,0,0;1,1,0,0,0,0;1,2,0,0,0,0;1,0,0,0,2,0;0,0,2,0,0,0;0,0,0,2,0,0;0,0,0,0,0,0;0,0,2,0,1,0;0,2,
0,0,1,0;0,3,0,0,1,0;0,3,1,1,0,0;0,0,1,0,0,1;0,0,0,0,0,0;0,0,3,1,0,0;3,3,8,0,0,0;2.69,2.7,7.38,0,0,0;3,2,6,0,0,0;
2,1,4,0,0,0;1,1,2,0,0,0;1,0,0,0,0,0];


    M=0;
    for j=1:9
        M(j)=cpm(e1,j);
    end
    atoms=0;
    for j=1:6
        atoms(j)=atomdatabase(e1,j);
    end
end


function [G,fugacity]=specie(n,T,T1,P,p0,x1,choice)


    a=x1(1);
    b=x1(2);
    c=x1(3);
```

```
d=x1(4);
Pc=x1(6);
Tc=x1(5);
H0=x1(7);
G0=x1(8);
ch=choice;
R=8.314;
syms TN
H=int(a+b*TN*10^(-3)+c*10^(-6)*TN^2+d*TN^(-2)*10^5,T,T1);
S=int(a/TN+b*10^(-3)+c*10^(-6)*TN+d*TN^(-3)*10^5,T,T1);
G=H0-T1/T*(H0-G0)+R*H-R*T1*S;

if ch==0                % Ideal Gas
   fugacity=0;
end

if (ch==1)              % RK
   [z,I,q,B]=genericcubiceos(ch,T1,P,Tc,Pc,x1(9));
   fugacity=z-1-log(z-B)-q*I;
end
if (ch==2)              % SRK
   [z,I,q,B]=genericcubiceos(ch,T1,P,Tc,Pc,x1(9));
   fugacity=z-1-log(z-B)-q*I;
end
if (ch==3)              % PR
   [z,I,q,B]=genericcubiceos(ch,T1,P,Tc,Pc,x1(9));
```

```
    fugacity=z-1-log(z-B)-q*I;
  end

  fugacity=exp(fugacity);                % the fugacity here refers to ln(fi)=GResidual/RT and I is G
residual
end

function [zv,Iv,q,B]=genericcubiceos(ch,T,P,Tc,Pc,w)
  R=8.314;
  mur=0;
  [alpha,sigma,epsi,omega,shi]=getvalueofeos(ch,T,Tc,w,mur);
  A=shi*alpha*R^(2)*Tc^(2)/Pc;
  b=omega*R*Tc/Pc;
  q=shi*alpha/omega*Tc/T;
  B=omega*P/Pc*(Tc/T);
  mat4=q*B^2+epsi*sigma*B^2*(1+B);
  mat3=(sigma*B*(1+B)+epsi*B*(1+B)-epsi*sigma*B^2-q*B);
  mat2=(1+B-sigma*B-epsi*B);
  mat1=-1;
  var=[mat1 mat2 mat3 mat4];
  z=roots(var);
  z=real(z);
  zv=max(z);
  Iv=1/(sigma-epsi)*log((zv+sigma*B)/(zv+epsi*B));
end
```

```
function [alpha,sigma,epsi,omega,shi]=getvalueofeos(ch,T,Tc,w,mur)
    mat=ones(3,5);                    % ch=1 for RK, ch=2 for SRK, ch=3 for PR
    mat(1,1)=(T/Tc)^(-0.5);
    mat(1,2)=1;
    mat(1,3)=0;
    mat(1,4)=0.08664;
    mat(1,5)=0.42748;
    mat(2,1)=(1+(0.480+1.574*w-0.176*w^2)*(1-(T/Tc)^(0.5)))^2;
    mat(2,2)=1;
    mat(2,3)=0;
    mat(2,4)=0.08664;
    mat(2,5)=0.42748;
    mat(3,1)=(1+(0.37464+1.574226*w-0.26692*w^2)*(1-(T/Tc)^(0.5)))^2;
    mat(3,2)=1+2^(0.5);
    mat(3,3)=1-2^(0.5);
    mat(3,4)=0.07779;
    mat(3,5)=0.45724;
    if ch<4
       mur=0;
    end
    mat(4,1)=(1+(0.406691+1.524095*w-0.158751*w^2-0.0003*mur)*(1-(T/Tc)^(0.5)))^2;
    mat(4,2)=1+2^(0.5);
    mat(4,3)=1-2^(0.5);
    mat(4,4)=0.07779;
    mat(4,5)=0.45724;
```

```
    alpha=mat(ch,1);
    sigma=mat(ch,2);
    epsi=mat(ch,3);
    omega=mat(ch,4);
    shi=mat(ch,5);
end



function [z,v]=newsolving(n,X,ta,moles,R,T1,phi,G,atom1,atoms,totatoms,P,p0,ch1)


    function G1 = func(X)
        Enj=0;
        for i=1:(n-1)
        Enj = Enj+X(i);
        end


        for i=1:(n-1)
            m(i)=(G(i)/R/T1 + log(phi(i)*X(i)/Enj*P/p0));
        end
%         m(n)=G(n)/R/T1;
         m(n) = G(n);
        G1 = sum(X.*m);


    end
```

```
Aeq=atoms;
beq=totatoms';



for i=1:n
   LB(i)=0;
end
options = optimset('Algorithm','sqp');
%z = fmincon(@func,X,[],[],Aeq,beq,LB,[],[],options);
z = fmincon(@func,X,[],[],Aeq,beq,LB,[],[],options);


v=0;


end


function [m5]=molematrix(atom1,newdata,totatoms)


[s1,s2]=size(atom1);
[s3,s4]=size(newdata);


m1=atom1;
m11=zeros(s1,s2);
m12=zeros(s1,s2);
m13=zeros(s1,s2);
```

```
m2=newdata;
m3=totatoms;
m4=m2';
% m5=zeros(s3,s4);
m21=zeros(s4,s3,s2);

for i=1:s4
   for j=1:s3

      for k=1:s2

         m21(i,j,k)=m4(i,j)*m1(i,k);

      end
   end

end
m24=zeros(1,s3,s2);
m24=sum(m21,1);

m23=zeros(s3,s2);
for i=1:s3
   for j=1:s2
   m23(i,j)=m24(1,i,j);
   end
```

```
end




for i=1:s4
   for j=1:s3


      for k=1:s2
         if m1(i,k)==0
            m11(i,k)=1;  %this will give atom3
            m12(i,k)=1;    % this will give atom4
         end
         if m1(i,k)~=0
            m11(i,k)=m1(i,k);       %atom3
            m12(i,k)=0;             %atom4
         end


         m4(i,j,k)=m21(i,j,k)/m23(j,k)/m11(i,k)*m3(k);









      end
   end
end
```

```
m41=zeros(s4,s3);


for i=1:s4
   for j=1:s3
      sum1=0;
      sum2=0;
      for k=1:s2
         sum1=sum1+m4(i,j,k);
         if m1(i,k)~=0
            sum2=sum2+1;
         end



      end
      if sum2==0
         sum2=1;
      end
      m41(i,j)=sum1/sum2;
   end
end
m5=m41';
end


function   [Ein]=energycalculator(x1,t11,n,m5,T,imole,ch1)
```

```
load('ENTHALPYDATAYAWS.mat');
l=1;
for loop=t11(1):t11(2):t11(3)
   sumforH0=0;                    % Calculates sum of Enthalpy of entering Streams
   sumforH1=0;                    % Calculates sum of Enthalpy of exiting Streams
   for i=1:n

      a= Enthalpydatabase(i,1);
      b= Enthalpydatabase(i,2);
      c= Enthalpydatabase(i,3);
      d= Enthalpydatabase(i,4);
      H0= Enthalpydatabase(i,5);
      T1=loop;
      syms TN
      R=8.314/1000;
      H1=c+b*T1+a*T1^2;

      %H1=int(a+b*TN*10^(-3)+c*10^(-6)*TN^2+d*TN^(-2)*10^5,T,T1);
%      H0=int(a+b*TN*10^(-3)+c*10^(-6)*TN^2+d*TN^(-2)*10^5,T,T);

      sumforH1=H1*m5(l,i)+H0*m5(l,i)+sumforH1;
      sumforH0=H0*imole(i)+sumforH0;
   end

   Ein(l)=sumforH1-sumforH0;
   l=l+1;
```

```
end
end


function write_gnuplot_file(t11,P,imole,m5,t,energy)
%UNTITLED5 Summary of this function goes here
%   Detailed explanation goes here
%% To write a file to use with Gnuplot
filename = sprintf('Plotfile_Temperature
Range_%1.1f_to_%1.1f_Pressure_%1.1f_FeedMole_ratios_CH4_H2O_O2_CO2_%3.3f_%3.3f_%3.3f_%
3.3f.txt', t11(1), t11(3), P, imole(1),imole(2),imole(3),imole(5));
A = [t';m5(:,1)';m5(:,2)';m5(:,3)';m5(:,4)';m5(:,5)';m5(:,6)';m5(:,7)';energy];
fileID = fopen(filename,'w');
fprintf(fileID,['### The Temperature Range is [%1.1f, %1.1f] K.\n' ...
'### The Pressure is %d bar.\n' ...
'### The Feed Ratio of CH4:H2O:O2:CO2 is [%1.1f :%1.1f :%1.1f :%1.1f] .\n' ...
'### %12s %15s %15s %15s %15s %15s %15s %15s %15s
\n'],t11(1),t11(3),P,imole(1),imole(2),imole(3),imole(5),
'Temperature','Methane','Water','Oxygen','Carbonmonoxide','Carbondioxide','Hydrogen','Carbon','Energy');
fprintf(fileID,'%15.4f %15.4f %15.4f %15.4f %15.4f %15.4f %15.4f %15.4f %15.4f \n',A);
fclose(fileID);
%%-------------------------------------------------------------------------



end
```

```
function write_gnuplot_file_HC_ratio(t11,P,imole,m5,HC)
%UNTITLED5 Summary of this function goes here
%   Detailed explanation goes here
%% To write a file to use with Gnuplot
filename = sprintf('Plotfile_Temperature
Range_%1.1f_to_%1.1f_Pressure_%1.1f_FeedMole_ratios_CH4_H2O_O2_CO2_%3.3f_%3.3f_%3.3f_%
3.3f.txt', t11(1), t11(3), P, imole(1),imole(2),imole(3),imole(5));
A = [];
fileID = fopen(filename,'w');
fprintf(fileID,['### The Temperature Range is [%1.1f, %1.1f] K.\n' ...
'### The Pressure is %d bar.\n' ...
'### The Feed Ratio of CH4:H2O:O2:CO2 is [%1.1f :%1.1f :%1.1f :%1.1f] .\n' ...
'### %12s %15s %15s %15s %15s %15s %15s %15s %15s
\n'],t11(1),t11(3),P,imole(1),imole(2),imole(3),imole(5),
'Temperature','Methane','Water','Oxygen','Carbonmonoxide','Carbondioxide','Hydrogen','Carbon','Energy');
fprintf(fileID,'%15.4f %15.4f %15.4f %15.4f %15.4f %15.4f %15.4f %15.4f %15.4f \n',A);
fclose(fileID);
%%-------------------------------------------------------------------------
 end
 function write_gnuplot_file_fugacitycoeff(t11,P,imole,m5,t,energy)
%UNTITLED5 Summary of this function goes here
%   Detailed explanation goes here
%% To write a file to use with Gnuplot
filename = sprintf('Plotfile_fugacity_Temperature
Range_%1.1f_to_%1.1f_Pressure_%1.1f_FeedMole_ratios_CH4_H2O_O2_CO2_%3.3f_%3.3f_%3.3f_%
3.3f.txt', t11(1), t11(3), P, imole(1),imole(2),imole(3),imole(5));
A = [t';m5(:,1)';m5(:,2)';m5(:,3)';m5(:,4)';m5(:,5)';m5(:,6)';m5(:,7)'];
```

```
fileID = fopen(filename,'w');
fprintf(fileID,['### The Temperature Range is [%1.1f, %1.1f] K.\n' ...
'### The Pressure is %d bar.\n' ...
'### The Feed Ratio of CH4:H2O:O2:CO2 is [%1.1f :%1.1f :%1.1f :%1.1f] .\n' ...
'### %12s %15s %15s %15s %15s %15s %15s %15s
\n'],t11(1),t11(3),P,imole(1),imole(2),imole(3),imole(5),
'Temperature','Methane','Water','Oxygen','Carbonmonoxide','Carbondioxide','Hydrogen','Carbon');
fprintf(fileID,'%15.4f %15.4f %15.4f %15.4f %15.4f %15.4f %15.4f %15.4f \n',A);
fclose(fileID);
%%-------------------------------------------------------------------------
 end
 function write_gnuplot_file_for_twelve_column_data(A)
%UNTITLED5 Summary of this function goes here
%   Detailed explanation goes here
%% To write a file to use with Gnuplot
filename =
sprintf('Plotfile_twelve_column_data_200C_to_400C_Pressure_9_FeedMole_ratios_CH4_H2O_O2_CO2
_1_1.0_0.0_1.txt');
 fileID = fopen(filename,'w');
fprintf(fileID,['### The Temperature Range is [200 , 400] C.\n' ...
'### The Pressure is 9 bar.\n' ...
'### The Feed Ratio of CH4:H2O:O2:CO2 is [1 : 0 : 0.50 : 1] .\n' ...
'### %12s %15s %15s %15s %15s %15s %15s %15s %15s %15s %15s %15s
\n'],'Temperature','Methane','Steam','Oxygen','Carbnmonoxi','Carbdioxi','Hydrogen','Carbon','H2/CO','CH4
% Con','CO2% Conv','Energy(KJ)');
fprintf(fileID,'%15.4f %15.4f %15.4f %15.4f %15.4f %15.4f %15.4f %15.4f %15.4f %15.4f %15.4f
%15.4f \n',A');
```

```
fclose(fileID);
%%-------------------------------------------------------------------------
 end
function write_gnuplot_file_for_thirteen_column_data(A,T,P,imole);
%UNTITLED5 Summary of this function goes here
%   Detailed explanation goes here
%% To write a file to use with Gnuplot
filename =
sprintf('thirteen_column_data/Plotfile_thirteen_column_data_%1.1f_to_%1.1f_Pressure_%1.1f_FeedMole
_ratios_CH4_H2O_O2_CO2_%2.2f_%2.2f_%2.2f_%2.2f.txt',T(1),T(3),P,imole(1),imole(2),imole(3),imol
e(5));
 fileID = fopen(filename,'w');
fprintf(fileID,['### The Temperature Range is [%1.1f , %1.1f] K.\n' ...
'### The Pressure is %1.1f bar.\n' ...
'### The Feed Ratio of CH4:H2O:O2:CO2 is [%1.1f : %1.1f : %1.1f : %1.1f] .\n' ...
'### %12s %15s %15s %15s %15s %15s %15s %15s %15s %15s %15s %15s %15s
\n'],T(1),T(3),P,imole(1),imole(2),imole(3),imole(5),'Temperature(C
)','Methane','Steam','Oxygen','Carbnmonoxi','Carbdioxi','Hydrogen','Carbon','H2/CO','CH4% Con','CO2%
Conv','H2O% Conv','Energy(KJ)');
fprintf(fileID,'%15.4f %15.4f %15.4f %15.4f %15.4f %15.4f %15.4f %15.4f %15.4f %15.4f %15.4f
%15.4f %15.4f\n',A');
fclose(fileID);
%%-------------------------------------------------------------------------
 end
 function write_gnuplot_file_for_pcentconvCO2(t11,P,imole,m5,t,energy)
%UNTITLED5 Summary of this function goes here
%   Detailed explanation goes here
```

```
%% To write a file to use with Gnuplot
filename =
sprintf('Plotfile_CO2_Percentage_Conversion_%1.1f_to_%1.1f_Pressure_%1.1f_FeedMole_ratios_CH4_
H2O_O2_CO2_%3.3f_%3.3f_%3.3f_%3.3f.txt', t11(1), t11(3), P, imole(1),imole(2),imole(3),imole(5));
A = [t,m5];
 fileID = fopen(filename,'w');
fprintf(fileID,['### The Temperature Range is [%1.1f, %1.1f] K.\n' ...
'### The Pressure is %d bar.\n' ...
'### The Feed Ratio of CH4:H2O:O2:CO2 is [%1.1f :%1.1f :%1.1f :%1.1f] .\n' ...
'### %12s %15s \n'],t11(1),t11(3),P,imole(1),imole(2),imole(3),imole(5), 'Temperature','Carbondioxide %
Conv');
fprintf(fileID,'%15.4f %15.4f \n',A');
fclose(fileID);
%%-------------------------------------------------------------------------
end
 function write_gnuplot_file_for_pcentconvCH4(t11,P,imole,m5,t,energy)
%UNTITLED5 Summary of this function goes here
%   Detailed explanation goes here
%% To write a file to use with Gnuplot
filename =
sprintf('Plotfile_CH4_Percentage_Conversion_%1.1f_to_%1.1f_Pressure_%1.1f_FeedMole_ratios_CH4_
H2O_O2_CO2_%3.3f_%3.3f_%3.3f_%3.3f.txt', t11(1), t11(3), P, imole(1),imole(2),imole(3),imole(5));
A = [t,m5];
 fileID = fopen(filename,'w');
fprintf(fileID,['### The Temperature Range is [%1.1f, %1.1f] K.\n' ...
'### The Pressure is %d bar.\n' ...
'### The Feed Ratio of CH4:H2O:O2:CO2 is [%1.1f :%1.1f :%1.1f :%1.1f] .\n' ...
```

```
'### %12s %15s \n'],t11(1),t11(3),P,imole(1),imole(2),imole(3),imole(5), 'Temperature','Methane %
Conv');
fprintf(fileID,'%15.4f %15.4f \n',A');
fclose(fileID);
%%------------------------------------------------------------------------
 end
 function write_gnuplot_file_for_pcentconvC(t11,P,imole,m5,t,energy)
%UNTITLED5 Summary of this function goes here
%   Detailed explanation goes here
%% To write a file to use with Gnuplot
filename =
sprintf('Plotfile_Carbon_Percentage_Conversion_%1.1f_to_%1.1f_Pressure_%1.1f_FeedMole_ratios_CH
4_H2O_O2_CO2_%3.3f_%3.3f_%3.3f_%3.3f.txt', t11(1), t11(3), P, imole(1),imole(2),imole(3),imole(5));
A = [t,m5];

fileID = fopen(filename,'w');
fprintf(fileID,['### The Temperature Range is [%1.1f, %1.1f] K.\n' ...
'### The Pressure is %d bar.\n' ...
'### The Feed Ratio of CH4:H2O:O2:CO2 is [%1.1f :%1.1f :%1.1f :%1.1f] .\n' ...
'### %12s %15s \n'],t11(1),t11(3),P,imole(1),imole(2),imole(3),imole(5), 'Temperature','Carbon % Conv');
fprintf(fileID,'%15.4f %15.4f \n',A');
fclose(fileID);
%%------------------------------------------------------------------------
 end
 function write_gnuplot_file_for_pcentconvCO2(t11,P,imole,m5,t,energy)
%UNTITLED5 Summary of this function goes here
```

```
%   Detailed explanation goes here
%% To write a file to use with Gnuplot
filename = sprintf('Plotfile_CO2 Percentage
Conversion_%1.1f_to_%1.1f_Pressure_%1.1f_FeedMole_ratios_CH4_H2O_O2_CO2_%3.3f_%3.3f_%3.
3f_%3.3f.txt', t11(1), t11(3), P, imole(1),imole(2),imole(3),imole(5));
A = [t,m5];
 fileID = fopen(filename,'w');
fprintf(fileID,['### The Temperature Range is [%1.1f, %1.1f] K.\n' ...
'### The Pressure is %d bar.\n' ...
'### The Feed Ratio of CH4:H2O:O2:CO2 is [%1.1f :%1.1f :%1.1f :%1.1f] .\n' ...
'### %12s %15s \n'],t11(1),t11(3),P,imole(1),imole(2),imole(3),imole(5), 'Temperature','Carbondioxide %
Conv');
fprintf(fileID,'%15.4f %15.4f \n',A');
fclose(fileID);
%%-------------------------------------------------------------------------
 end
 function write_gnuplot_file_for_fugacitycoeffmix_EOS(A)
%UNTITLED5 Summary of this function goes here
%   Detailed explanation goes here
%% To write a file to use with Gnuplot
filename =
sprintf('Plotfile_Mixture_fugacity_coefficient_200_C_to_1200_C_Pressure_20_bar_FeedMole_ratios_CH
4_H2O_O2_CO2_1_0.6_0.1_0.6_EOS.txt');
%A = [t,m5];
 fileID = fopen(filename,'w');
fprintf(fileID,['### The Temperature Range is [200 , 1200] Celcius.\n' ...
'### The Pressure is 20 bar.\n' ...
```

```
'### The Feed Ratio of CH4:H2O:O2:CO2 is [1 :0.6 :0.1 :0.6] .\n' ...
'### %12s %15s %15s %15s %15s \n'], 'Temperature','Ideal', 'RK', 'SRK', 'PR');
fprintf(fileID,'%15.4f %15.4f %15.4f %15.4f %15.4f \n',A');
fclose(fileID);
%%-------------------------------------------------------------------------
 end
 function write_gnuplot_file_for_fugacitycoeffmix(t11,P,imole,m5,t,energy)
%UNTITLED5 Summary of this function goes here
%   Detailed explanation goes here
%% To write a file to use with Gnuplot
filename =
sprintf('Plotfile_Mixture_fugacity_coefficient_%1.1f_to_%1.1f_Pressure_%1.1f_FeedMole_ratios_CH4_
H2O_O2_CO2_%3.3f_%3.3f_%3.3f_%3.3f.txt', t11(1), t11(3), P, imole(1),imole(2),imole(3),imole(5));
A = [t,m5];
 fileID = fopen(filename,'w');
fprintf(fileID,['### The Temperature Range is [%1.1f, %1.1f] K.\n' ...
'### The Pressure is %d bar.\n' ...
'### The Feed Ratio of CH4:H2O:O2:CO2 is [%1.1f :%1.1f :%1.1f :%1.1f] .\n' ...
'### %12s %15s \n'],t11(1),t11(3),P,imole(1),imole(2),imole(3),imole(5), 'Temperature',',Mixture
Fugacity');
fprintf(fileID,'%15.4f %15.4f \n',A');
fclose(fileID);
%%-------------------------------------------------------------------------
 end
```

FOR KINETIC STUDY:

```
clear;
```

```
%% This code file is the main reformer bed script
% brief introduction explaining the reason for them.
%% This complete code will have the following use(s):
% 1) Simulation of Pseudo homogeneous fixed bed reformer
% 2) To be able to simulate the SRM/DRM both individually and
% in combined mode.
 %% SIMULATION BEGINS:
% Call for properties from the database function:
 [D, W_F0, T0, P0, dp, E_s, tau, rho_b, E_b]= reactor_database();
 % Kinetics:
% This code uses the following kinetic models:
%   1) Steam reforming of methane LHHW model using : J. Xu et al., AIChE Journal, 1989, 35, 88.
%   2) Dry reforming of methane LHHW model using : X. E. Verykios et al., International journal of
Hydrogen Energy, 2003, 28, 1045.
 % Chemical reactions involved :
%   1) CH4 + 2H2O <---> 3H2 + CO
%   2) CO + H2O <---> H2 + CO2
%   3) CH4 + 2H2O <---> 4H2 + CO2
%   4) CH4 + CO2 <---> 2H2 + 2CO
%% Using solver script :
 % Model selection choices:
% 1) choice 1 : SRM
% 2) choice 2 : DRM
% 3) choice 3 : SRM+DRM
dt=0.0795;      %m
At=pi/4*dt^2;   % m^2
mod_sel=3;
```

```
rho_b = 946800;     %g/m^3
 [o1, o2] = solver_script(mod_sel,D, W_F0, T0, dp, E_s, tau, rho_b, E_b);
o1=o1/(rho_b*At);
%Temperature Profile
figure;
subplot(2,1,1);
plot(o1, o2(:,7));
xlabel('bed length, m');
ylabel('Temperature K');
%
subplot(2,1,2);
plot(o1, o2(:,(1:6)));
xlabel('bed length, m');
ylabel('mole/hr');
 legend('CO','H_2O','CO_2','H_2','He','CH_4');
%
function [o1 , o2]= solver_script(mod_sel,D, W_F0, T0, P0, dp, E_s, tau, rho_b, E_b)
 lspan=[0:1:1000];
% a = CO
% b = H2O
% c = CO2
% d = H2
% e = He
% f = CH4
if mod_sel==1 % SRM is chosen as kinetic model
    initials=[0.00001,5,0.00001,0.00001,0.00001,5,1273];   %  following order :
[CO,H2O,CO2,H2,He,CH4,T] This is to fix the feed mole ratio entering the reactor
```

```
    [o1 , o2]=ode15s('SRM',lspan,initials);
end
 if mod_sel==2 % DRM is chosen as kinetic model
    initials=[0.00001,0.00001,1,0.00001,0.00001,1];   %  following order : [CO,H2O,CO2,H2,He,CH4]
This is to fix the feed mole ratio entering the reactor
    [o1 , o2]=ode45('DRM',lspan,initials);
end
 if mod_sel==3 % SRM+DRM is chosen as kinetic model
    initials=[0.00001,100,100,0.00001,0.00001,150,1173,28.37];   %  following order :
[CO,H2O,CO2,H2,He,CH4,T] This is to fix the feed mole ratio entering the reactor
    [o1 , o2]=ode15s('SRM_DRM_rev1',lspan,initials);
end
 % if mod_sel==3 % SRM+DRM is chosen as kinetic model
%     initials=[0.00001,1000,1000,0.00001,0.00001,1273];   %  following order :
[CO,H2O,CO2,H2,He,CH4,T] This is to fix the feed mole ratio entering the reactor
%     [o1 , o2]=ode15s('SRM_DRM_rev2',lspan,initials);
% end
 end
function dfdw=SRM_DRM_rev1(~,F)
Fco=F(1);
Fh2o=F(2);
Fco2=F(3);
Fh2=F(4);
Fhe=F(5);
Fch4=F(6);
P1 = F(8);     % partial pressures in bar
T= F(7);
```

```
R=8.314;        % Universal gas constant Pa.m3/mol/K
Ftot=F(1)+F(2)+F(3)+F(4)+F(5)+F(6);
P(1) = P1*F(1)/Ftot;
P(2) = P1*F(2)/Ftot;
P(3) = P1*F(3)/Ftot;
P(4) = P1*F(4)/Ftot;
P(5) = P1*F(5)/Ftot;
P(6) = P1*F(6)/Ftot;
% Steam reforming LHHW parameters using Xu and Froment (1989) expressions
K1=exp(30.420-27106/T);
K2=exp(-3.798+4160/T);
K3=exp(34.218-31266/T);
%
KCH4=6.65e-4*exp(38280/8.314/T);
KCO=8.23e-5*exp(70650/8.314/T);
KH2=6.12e-9*exp(82900/8.314/T);
KH2O=1.77e5*exp(-88680/8.314/T);
%
kin1=4.2248e15*exp(-240100/8.314/T);
kin2=1.955e6*exp(-67130/8.314/T);
kin3=1.0202e15*exp(-243900/8.314/T);
%
DEN=1+KCH4*P(6)+KCO*P(3)+KH2*P(4)+KH2O*P(2)/P(4);
% Dry reforming LHHW parameters using Verykios (2003) expressions
K1_k2 = 2.61*10^(-1)*exp(-4300/T)*3600;
K_3 = 5.17*10^(-3)*exp(8700/T);
k_4 = 5.35*10^(-1)*exp(-7500/T)*3600;
```

```
%
r1=kin1/P(4)^2.5/DEN^2*(P(6)*P(2)-P(4)^3*P(1)/K1);
r2=kin2/P(4)/DEN^2*(P(1)*P(2)-P(4)*P(3)/K2);
r3=kin3/P(4)^3.5/DEN^2*(P(6)*P(2)^2-P(4)^4*P(3)/K3);
r4 = (K1_k2*K_3*k_4*P(6)*P(3)/(K1_k2*K_3*P(6)*P(3)+K1_k2*P(6)+K_3*k_4*P(3)));
 Dh1=535655+R*(4.4810*(T-298.15)-0.0102*((T-298.15)^2)/2+2.164e-06*((T-298.15)^3)/3+2400*(1/T-
1/298.15));
Dh2=2846+R*(1.86*(T-298.15)-0.00054*((T-298.15)^2)/2+0*((T-298.15)^3)/3+116400*(1/T-1/298.15));
Dh3=252671+R*(9.811*(T-298.15)-0.009248*((T-298.15)^2)/2+2.164e-06*((T-
298.15)^3)/3+106700*(1/T-1/298.15));
Dh4=246979+R*(6.091*(T-298.15)-0.008168*((T-298.15)^2)/2+2.164e-06*((T-
298.15)^3)/3+126100*(1/T-1/298.15));
 cp1=R*(3.37600000000000*((T-298.15))+0.000557000000000000*((T^2-298.15^2))/2+0*((T^3-
298.15^3))/3-3100*(1/T-1/298.15));
cp2=R*(3.47000000000000*((T-298.15))+0.00145000000000000*((T^2-298.15^2))/2+0*((T^3-
298.15^3))/3+12100*(1/T-1/298.15));
cp3=R*((T-298.15)+5.45700000000000*((T-298.15))+0.00104500000000000*((T^2-
298.15^2))/2+0*((T^3-298.15^3))/3-115700*(1/T-1/298.15));
cp4=R*(3.24900000000000*((T-298.15))+0.000422000000000000*((T^2-298.15^2))/2+0*((T^3-
298.15^3))/3+8300*(1/T-1/298.15));
cp5=R*(3.63980000000000*((T-298.15))+0.00340000000000000*((T^2-
298.15^2))/2+2.00000000000000e-06*((T^3-298.15^3))/3+0*(1/T-1/298.15));
cp6=R*(1.70200000000000*((T-298.15))+0.00908100000000000*((T^2-298.15^2))/2-
2.16400000000000e-06*((T^3-298.15^3))/3+0*(1/T-1/298.15));
 %U=HTP(T);    % j/m2.hr.K
U=350;          %http://www.engineersedge.com/thermodynamics/overall_heat_transfer-table.htm
Tr=1173;        %K
```

```
dt=0.0795;      %m
At=pi/4*dt^2;   % m^2
rho_g = P1*10^5/(Fco*28+Fh2o*18+Fco2*44+Fco2+Fh2*2+Fhe*4+Fch4*16)/Ftot/(R*T);
u_s = (Fco*28+Fh2o*18+Fco2*44+Fco2+Fh2*2+Fhe*4+Fch4*16)/Ftot*rho_g/At;
rho_b = 946800;     %g/m^3
Cp= (Fco*cp1+Fh2o*cp2+Fco2*cp3+Fco2+Fh2*cp4+Fhe*cp5+Fch4*cp6)/Ftot; % j/(mol.K)
dfdw(1,1)=(r1-r2+2*r4);
dfdw(2,1)=-(r1+r2+2*r3);
dfdw(3,1)=(r2+r3-r4);
dfdw(4,1)=(3*r1+r2+4*r3+2*r4);
dfdw(5,1)=0;
dfdw(6,1)=-(r1+r3+r4);
%dfdl(7,1)=(-1*(r1*Dh(1)+r2*Dh(2)+r3*Dh(3)+r4*Dh(4))*rho_b-4*U/dt*(T-
Tr))/(u_s*rho_g*(sum(F(1:6).*cp(1:6)')/sum(F(1:6).*M(1:6)')));
%dfdl(7,1)=(-1*(r1*Dh(1)+r2*Dh(2)+r3*Dh(3)+r4*Dh(4))*rho_b)/(u_s*rho_g*Cp);
dp=17.41/1000;
a=6/dp;
dfdw(7,1)= -(r1*Dh1+r2*Dh2+r3*Dh3+r4*Dh4)/(Cp*Ftot)*1000+U*a*(Tr-T)/rho_b;
%dfdw(7,1)= -(r1*Dh1+r2*Dh2+r3*Dh3+r4*Dh4)/(Cp*Ftot)*1000;
% G=rho_g*u_s;
% phi=0.5319;
% mu=viscosity(F);
% beta0=G*(1-phi)/(rho_g*dp*phi^3)*(150*(1-phi)*mu/dp+1.75*G);
% dfdw(8,1)=-beta0/(At*rho_b);
 G=rho_g*u_s;
phi=0.5319;
mu=viscosity(F);    %Pa.S
```

```
beta0=G/(3600000)*(1-phi)/(rho_g*(1/1000)*dp*phi^3)*(150*(1-phi)*mu/dp+1.75*G/(3600000));
%pa/m
dfdw(8,1)=-beta0/(At*rho_b)/100000;          %bar/g
 end
function dfdl=SRM(l,F)
% feed conditions
% a = CO
% b = H2O
% c = CO2
% d = H2
% e = He
% f = CH4
 % Rearranging the order of species
% F_dummy(1)=F(3);
% F_dummy(2)=F(2);
% F_dummy(3)=F(4);
% F_dummy(4)=F(5);
% F_dummy(5)=F(6);
% F_dummy(6)=F(1);
%
% F = F_dummy;
R=8.314;
eta1=1;
eta2=1;
eta3=1;
eta4=1;
% partial pressures in bar
```

```
Ptot0 = 28.37;
% temperatures in K
% T = 1000;
%
Ftot=F(1)+F(2)+F(3)+F(4)+F(5)+F(6);
P(1) = Ptot0*F(1)/Ftot;
P(2) = Ptot0*F(2)/Ftot;
P(3) = Ptot0*F(3)/Ftot;
P(4) = Ptot0*F(4)/Ftot;
P(5) = Ptot0*F(5)/Ftot;
P(6) = Ptot0*F(6)/Ftot;
 K1=exp(30.420-27106/F(7));
K2=exp(-3.798+4160/F(7));
K3=exp(34.218-31266/F(7));
%
KCH4=6.65e-4*exp(38280/8.314/F(7));
KCO=8.23e-5*exp(70650/8.314/F(7));
KH2=6.12e-9*exp(82900/8.314/F(7));
KH2O=1.77e5*exp(-88680/8.314/F(7));
%
kin1=4.2248e15*exp(-240100/8.314/F(7));
kin2=1.955e6*exp(-67130/8.314/F(7));
kin3=1.0202e15*exp(-243900/8.314/F(7));
%
DEN=1+KCH4*P(6)+KCO*P(3)+KH2*P(4)+KH2O*P(2)/P(4);
r1=kin1/P(4)^2.5/DEN^2*(P(6)*P(2)-P(4)^3*P(1)/K1);
r2=kin2/P(4)/DEN^2*(P(1)*P(2)-P(4)*P(3)/K2);
```

```
r3=kin3/P(4)^3.5/DEN^2*(P(6)*P(2)^2-P(4)^4*P(3)/K3);
%
load('specie_data');
for i=1:6
T1=F(7);
cp(i)=double(R*(specie_data(i,2)+specie_data(i,3)*T1+specie_data(i,4)*T1^2+specie_data(i,5)*T1^(-
2)));
end
%
%
load('rxn_data');
syms T
for i=1:4
 dh(i)=rxn_data(i,1)+R*double(int(rxn_data(i,2)+rxn_data(i,3)*T+rxn_data(i,4)*T^2+rxn_data(i,5)*T^(-
2),T,298.15,F(7)));


end
%
U=HTP(F(7));          %
Tr=900;         %K
dt=0.0978;      %m
At=pi/4*dt^2;   % m^2
G=0.003953;     %g.mol/hr
rhob=1.362;     %g/m^3
Cp=sum(cp(1:6).*F(1:6)')/sum(F(1:6));
dfdl(1,1)=(r1-r2)/(At*rhob);
```

```
dfdl(2,1)=(-(r1+r2+2*r3))/(At*rhob);

dfdl(3,1)=(r2+r3)/(At*rhob);

dfdl(4,1)=(3*r1+r2+4*r3)/(At*rhob);

dfdl(5,1)=0;

dfdl(6,1)=(-(r1+r3))/(At*rhob);

%dfdw(7,1)=(-1*(dh(1)*eta1*r1+dh(2)*eta2*r2+dh(3)*eta3*r3)-4*U*(F(7)-

Tr)/dt)/(F(1)*cp(1)+F(2)*cp(2)+F(3)*cp(3)+F(4)*cp(4)+F(5)*cp(5)+F(6)*cp(6));

dfdl(7,1)=1/(G*Cp)*(4*U*(Tr-F(7))/dt-(dh(1)*eta1*r1+dh(2)*eta2*r2+dh(3)*eta3*r3)*rhob);

end
```